Programmable control of nucleation for algorithmic self-assembly

Rebecca Schulman[1,*] and Erik Winfree[1,2,†]

[1]*Department of Computation and Neural Systems, California Institute of Technology, Pasadena, CA 91125, USA*

[2]*Department of Computer Science, California Institute of Technology, Pasadena, CA 91125, USA*

(Dated: July 13, 2006)

Algorithmic self-assembly, a generalization of crystal growth processes, has been proposed as a mechanism for autonomous DNA computation and for bottom-up fabrication of complex nanostructures. A 'program' for growing a desired structure consists of a set of molecular 'tiles' designed to have specific binding interactions. A key challenge to making algorithmic self-assembly practical is designing tile set programs that make assembly robust to errors that occur during initiation and growth. One method for the controlled initiation of assembly, often seen in biology, is the use of a seed or catalyst molecule which reduces an otherwise large kinetic barrier to nucleation. Here, we show how to program algorithmic self-assembly similarly, such that seeded assembly proceeds quickly, but there is an arbitrarily large kinetic barrier to unseeded growth. We demonstrate this by introducing a family of tile sets for which we rigorously prove that, under the right physical conditions, increasing the size of the tile set by a constant amount exponentially reduces the rate of spurious nucleation. Simulations of these 'zig-zag' tile sets suggest that under plausible experimental conditions, it is possible to grow seeded crystals in just a few hours such that less than 1 percent of crystals are spuriously nucleated. Simulation results also suggest that zig-zag tile sets could be used for detection of single DNA strands. Along with prior work on constructing tile sets that are robust to assembly errors during growth, this work is a step toward understanding how algorithmic self-assembly can be performed with low error rates without a significant reduction in assembly speed.

I. INTRODUCTION

Molecular self-assembly is an emerging low-cost alternative to lithography for the creation of materials and devices with sub-nanometer precision [1, 2]. Whereas top-down methods such as photolithography impose order externally (e.g. a mask with a blueprint of the desired structure) bottom-up fabrication by self-assembly requires that this information be embedded within the chemical processes themselves.

Biology demonstrates that self-assembly can be used to create complex objects in this way. Organisms produce sophisticated and functional organization from the nanometer scale to the meter scale and beyond. Structures such as virus capsids, bacterial flagella, actin networks and microtubules can assemble from their purified components, even without external direction from enzymes or metabolism. This suggests that spontaneous molecular self-assembly can be engineered to create an interesting class of complex supramolecular structures. A central challenge is how to create a large structure without having to design a large number of unique molecular components.

Algorithmic self-assembly has been proposed as a general method for engineering such structures [3] by making use of local binding affinities to direct the placement of molecules during growth. The binding of a particular molecule at a particular site is viewed as a computational or information transfer step. By designing only a modest number of molecular species, which constitute the instructions or program for how to grow an object, complex objects can be constructed in principle [4, 5]. The implementation of algorithmic self-assembly requires controlled nucleation : An assembly that grows from the right nucleus executes the instructions for assembly in the correct order, while uncontrolled nucleation leads to a spectrum of undesired products. The primary concern of this paper is how to engineer molecules that ensure self-assembly begins with controlled nucleation. We address this question theoretically, using a model that is commonly used to study crystallization [6], but which incorporates the particularities of algorithmic self-assembly.

To motivate the model we use, we first describe a specific molecular system that can implement algorithmic self-assembly experimentally. DNA double crossover molecules [7] and related complexes [8, 9, 10, 11, 12] (henceforth, 'DNA tiles') have the necessary regular structure and programmable affinity to implement algorithmic self-assembly, and simple periodic [8, 13] and algorithmic [14, 15, 16] self-assembly reactions have been realized experimentally. As an example, consider a DNA double crossover molecule shown in Figure 1, which self-assembles from 4 strands of synthetic DNA whose sequences have been designed such that the desired pseudoknotted configuration maximizes the Watson-Crick complementarity [17, 18]. Since the energy landscape for folding is dominated by logical complementarity more so than by specific sequence details, it is possible to design similar double crossover molecules with completely dis-

*Electronic address: rebecka@caltech.edu

†Electronic address: winfree@dna.caltech.edu

similar sequences. To date, nearly 100 different molecules of this type have been synthesized.

Interactions between DNA tiles are dictated by the base sequences of each of four single-stranded overhangs, termed 'sticky ends,' which can be chosen as desired for each tile type. Tiles assemble through the hybridization of complementary sticky ends. The free energy of association for two tiles in a particular orientation is assumed to be dominated by the energy of hybridization between their adjacent sticky ends, which is favorable when complementary sticky ends bind, but negligible or unfavorable for non-complementary sticky ends. The DNA tiles shown crystallize into sheets via the binding of sticky ends to four adjacent molecules, forming a lattice (Figure 1). When multiple tile types are present in solution, each site on the growth front of the crystal preferentially will select from solution a tile that makes the most favorable bonds. For example, under appropriate physical conditions, a tile that can attach by two sticky ends will be secured in place, while tiles that attach by only a single sticky end usually will be rejected due to a fast dissociation reaction. We call these 'favorable' and 'unfavorable' attachments, respectively.

The design of an algorithmic self-assembly reaction begins with the creation of a tile program and its evaluation in an idealized model of tile interaction, the abstract tile assembly model (aTAM) [19]. A DNA tile is represented as a square tile, with labels on each side representing the four sticky ends. Polyomino tiles with labels on each unit-length of the perimeter can be used in addition to square tiles, since it is possible to generate the corresponding DNA structures. A tile program consists of a set of such tiles, the strength with which each possible pair of labels binds, a designated seed tile, and a strength threshold τ. Under the aTAM, growth starts with a designated assembly of tiles (usually just the seed tile) and proceeds by allowing favorable attachments of tiles to occur. That is, tiles may be added where the total strength of the connections between the tile and the assembly is greater than or equal to the threshold τ. Addition of tiles is irreversible, but at a given step, any allowed attachment may be performed. An example of a structure that can be constructed using algorithmic self-assembly, a Sierpinski triangle, is shown in Figure 2. Beginning with the seed tile, assembly in the aTAM will result in the growth of an V-shaped boundary that is subsequently (and simultaneously) filled in by 'rule tiles' that obtain their input from their bottom sides, presenting their output on their top sides. The four rule tiles for this self-assembly program consist of the four cases in the look-up table for XOR, thus implementing the standard iterative procedure for building Pascal's triangle mod 2. Tile sets for the construction of a variety of desired products have been described [3, 20, 21, 22, 23, 24], including a tile set capable of universal construction [5].

In contrast to assembly in the aTAM, the assembly of DNA tiles is neither errorless nor irreversible, nor is it guaranteed to start from a seed tile. For example, in recent experimental demonstrations of algorithmic self-assembly [15, 16], between 1% and 10% of tiles mismatched their neighbors and only a small fraction of the observed crystals were properly nucleated from seed molecules. Following [25], Figure 3 illustrates how unseeded nucleation and unfavorable attachments can lead to undesired assemblies.

To theoretically study the rates at which errors occur, we need a model that includes energetically unfavorable events. The kinetic Tile Assembly Model (kTAM) [19] describes the dynamics of assembly according to an inclusive set of reversible chemical reactions: a tile can attach to an assembly anywhere that it makes even a weak bond, and any tile can dissociate from the assembly at a rate dependent on the total strength with which it adheres to the assembly (see Figure 4). The kinetic tile assembly model is a lattice-based model, in which free tiles are assumed to be well mixed, and effects within the crystal such as bending or pressure differences are ignored. The kTAM has been used to study the trade-off between crystal growth rate and the frequency of mismatches (errors) in seeded assemblies [19]. Analysis of assembly within the kTAM also suggests that it is possible to control assembly errors by reprogramming an existing tile set so as to introduce redundancy. 'Proofreading tile sets' [26, 27, 28, 29] transform a tile set by replacing each individual tile with a $k \times k$ block of tiles, exponentially reducing seeded growth errors with respect to the size of the block.

In this paper we propose a related method to control nucleation errors without significant slow-down. This method exponentially reduces the rate at which assemblies without a seed tile grow large (unseeded growth), while maintaining the rate of growth that starts from a seed tile and proceeds roughly according to aTAM (seeded growth). To do so, a tile set must satisfy two conflicting constraints: when assembly begins from a seed tile, it must proceed quickly, whereas assembly that starts from a non-seed tile must overcome a barrier to nucleation in order to continue.

How is it possible to have a barrier to nucleation only when no seed is present? In a mechanism for the control of 1-dimensional polymerization, found both in biology [30, 31] and engineering [32], a seed induces a conformational or chemical change to monomers, without which monomers cannot polymerize. For example, in spontaneous actin polymerization, it is proposed that a trimer occasionally bends to form an incipient helix that allows for further nucleation [30], but the Arp 2/3 protein complex (potentially among others) imitates the shape of an unfavorable intermediate [33]. In two and three dimensional systems – condensation of a gas [34], crystallization [35], or in general in the Ising model [36], classical nucleation theory [37, 38] predicts that a barrier to nucleation exists because clusters have a unfavorable energies proportional to the surface area of the cluster (possibly due to interfacial tension or pressure differences with respect to the surrounding solution), and favorable ener-

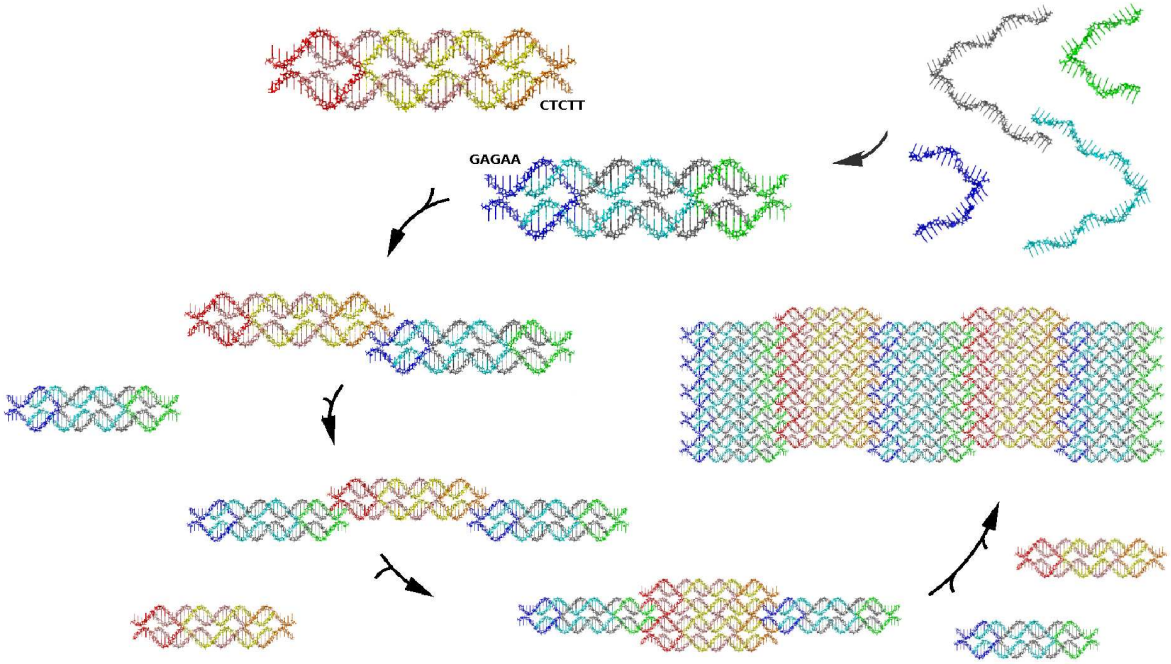

FIG. 1: **A DNA double crossover molecule and its assembly into a 2D crystal.**

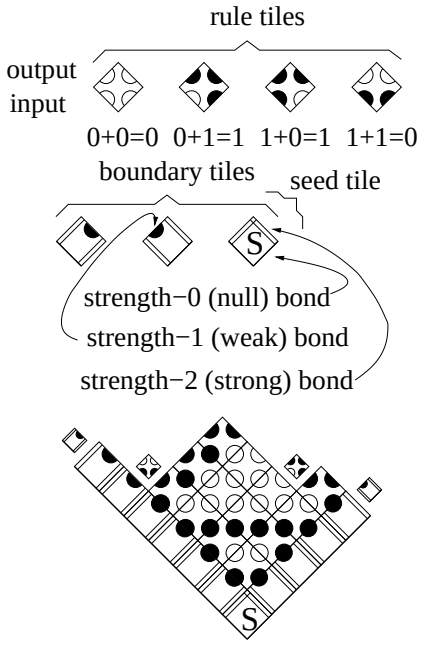

FIG. 2: **The Sierpinski tile set.** Because DNA tiles are generally not rotationally symmetric, formal tiles cannot be rotated. The lower diagram shows the seeded growth of the Sierpinski tiles according to the aTAM at $\tau = 2$. The small tiles indicate the (only) four sites where growth can occur. At each location exactly one tile matches both exposed sides, so assembly results in a unique pattern.

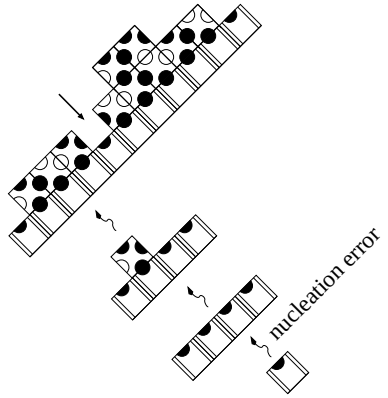

FIG. 3: **Errors resulting from improper nucleation.** Tile sets containing rule tiles and boundary tiles of the sort used by the tile set in Figure 2 are particularly prone to nucleation errors. Improper nucleation can produce a long facet where a single insufficient attachment can allow several adjacent tiles to attach favorably. These blocks of tiles may be incompatible, leading to an inevitable mismatch at their intersection. An example of a site where such a mismatch will occur is pointed to by the straight arrow.

gies proportional to the volume of the cluster. Because volume grows more quickly than surface area as clusters grow larger, a supersaturated regime exists where small clusters tend to melt, but above a critical size, cluster

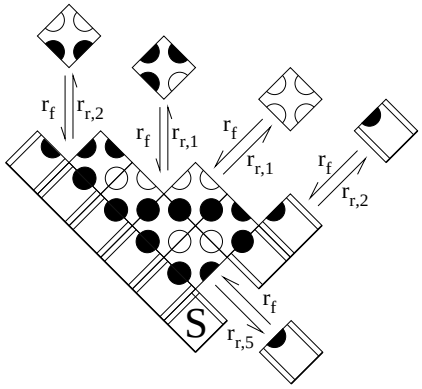

FIG. 4: **The kinetic Tile Assembly Model (kTAM).** For the growth of an isolated crystal under unchanging tile concentrations, the forward (association) rate in the kTAM is $r_f = k_f[tile] = k_f e^{-G_{mc}}$, while the reverse (dissociation) rate is $r_{r,b} = k_f e^{-bG_{se}}$ for a tile that makes bonds with total strength b. Parameters G_{mc} and G_{se} govern monomer tile concentration and sticky-end bond strength, respectively. A representative selection of possible events is shown here. Attachments with reverse rates $r_{r,1}$ are unfavorable for $G_{mc} > G_{se}$. The kTAM approximates the aTAM with threshold τ when $G_{mc} = \tau G_{se} - \epsilon$, in which case the same set of reactions are favorable or unfavorable in the two models.

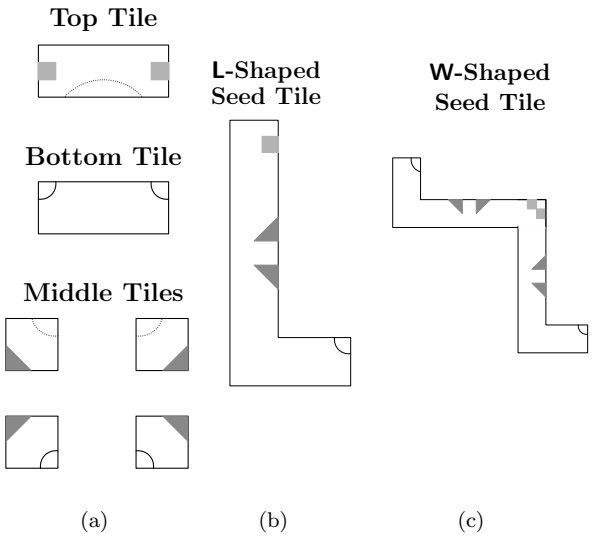

FIG. 5: **The width 4 zig-zag tile set and seed tiles.** **(a)** Zig-zag tiles. Each shape represents a single tile. Tiles have matching bonds of strength 1 when the shapes on their edges match. **(b)** The L-shaped seed nucleates linear assemblies. **(c)** The W-shaped seed tile, with appropriate tiles for vertical zig-zag growth, could nucleate V-shaped assemblies.

growth rather than melting is favored. Aspects of both these methods are combined in some crystalline ribbons or tubes, where growth, initially in two dimensions, is disfavored because of unfavorable surface area/volume interactions, up to the point that the full width ribbon or tube has been formed. A seed structure allows immediate growth by providing a stable analogue to a full-width assembly. Protein microtubules [39] and DNA tubes [40, 41, 42] exhibit this type of nucleation barrier.

In this paper we describe a tile set, the zig-zag tile set, that uses this method for the control of nucleation during algorithmic self-assembly. Zig-zag tiles assemble into a potentially long ribbon of predefined width. While a seed tile allows zig-zag ribbons to grow immediately, only full-width boundaries can grow by favorable attachments, so without the seed tile there is a critical size barrier that prevents spurious nucleation. Because it is simple to reengineer the monomers used in self-assembly, by redesigning the tile set it is possible to increase the width and therefore the critical size.

In addition to its intrinsic interest as an engineering scheme for controlling nucleation, the zig-zag tiles solve the aforementioned problem in controlling nucleation during algorithmic growth. With an appropriate seed, zig-zag ribbons can play the same role as the V-shaped boundary in Figure 2. Since rule tiles are not likely to spuriously nucleate on their own under optimal assembly conditions [19], once this boundary has set up the correct initial information, algorithmic self-assembly will proceed with few spurious side products.

In Section II, we describe the zig-zag tile set family in detail. In Section III, we explain a mass-action model of self-assembly kinetics. In Section IV we analyze thermodynamic constraints on ribbon growth. In Section V, we prove our main theorem, that the rate of spurious nucleation decreases exponentially with the width of the zig-zag tile set. In contrast, the speed of seeded assembly decreases only linearly with width. Thus, for a given volume, we can construct a tile set such that no spurious nucleation is expected to occur during assembly. This illustrates how the logical redesign of molecules can be qualitatively more effective in preventing undesired nucleation than just controlling physical quantities such as temperature and monomer concentration. In Section VI, we use both mass-action and stochastic simulations to provide numerical estimates of nucleation rates, which suggest that reasonably sized zig-zag tile sets can be expected to be effective in the laboratory.

II. THE ZIG-ZAG TILE SET

A self-assembly program is a set of tiles that accomplishes a given task.

A **zig-zag tile set** (Figure 5(a)) of width k contains tiles that assemble to form a periodic ribbon of width k (Figure 6). Zig-zag tile sets of widths $k \geq 2$ can be constructed. A zig-zag tile set includes a **top tile** and a **bottom tile**, each consisting of 2 horizontally connected

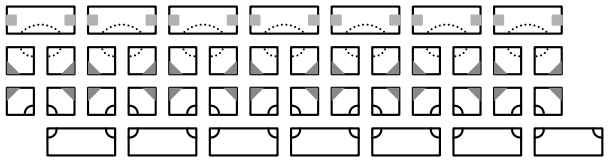

FIG. 6: **A zig-zag assembly.** The ribbon structure formed by the zig-zag tile set.

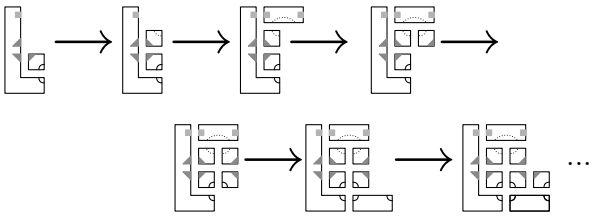

FIG. 7: **Seeded Growth.** Seeded growth of a zig-zag tile set in the aTAM. The same growth pattern occurs reversibly in the kTAM when $G_{mc} = 2G_{se} - \epsilon$.

square tiles. Each of the $k-2$ rows between the top and bottom tiles contains two unique **middle tiles** that alternate horizontally. Having distinct tiles in alternating columns enforces the staggering of the top and bottom tiles. Each tile label has exactly one match on another tile type, so that the tiles cannot assemble to form any other structures held together by sticky end bonds.

The tile set is designed to operate in a physical regime where the attachment of a tile to another tile or assembly by two matching sides is energetically favorable, whereas an attachment by only one bond is energetically unfavorable. In this physical regime, algorithmic self-assembly is possible. In the aTAM, these conditions translate to growth with a threshold of 2. Growth beginning from any tile in the zig-zag tile set goes nowhere in the aTAM : no two tiles can join by at least two bonds. Instead, a seed tile can be used to initiate growth. Figures 5(b) and 5(c) show two possible seed tiles : an L-shaped **seed tile** consisting of k vertically connected square tiles and a square tile horizontally connected to the bottom of the vertical connected tiles and a similar W-shaped seed tile. Figure 7 illustrates the only possible growth path in the aTAM from the L-shaped seed. The staggering of the top and bottom tiles allows growth to continue indefinitely along a zig-zag path. (This growth path is analogous to spiral growth in microtubules but unwrapped onto the plane.) Note that the top and bottom tiles alternately provide the only way to proceed to each successive column. Assemblies that do not span the full width (k tiles) cannot bind both kinds of tiles, and thus cannot grow indefinitely. Growth from a seed tile of less than full width would stall. For example, with a seed tile of width $k-1$, the top tile could not attach by two bonds to the assembly.

In the kTAM, seeded growth occurs in the same pattern as in the aTAM. Unlike in the aTAM, however, there

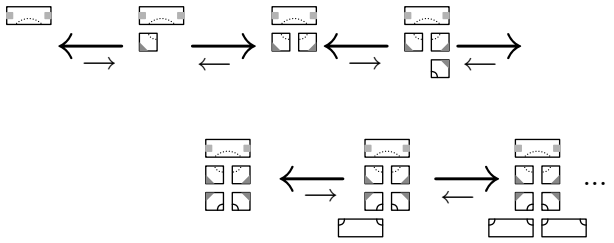

FIG. 8: **Unseeded Growth.** A possible series of steps by which the tiles could spuriously nucleate in the kTAM.

are also series of reactions that can produce a full width assembly in the absence of a seed tile. The formation of such an assembly is called a spurious nucleation error. An example of such unseeded growth is shown in Figure 8. Under the conditions of interest, some steps in spurious nucleation are energetically favorable, but at least $k-1$ must be unfavorable before the full-with assembly is formed. At this point, further growth is favorable. Spurious nucleation is a transition from assembly *melting*, where assemblies are more likely to fall apart than they are to get larger, to assembly *growth*, where each assembly step is energetically favorable. Any assembly where melting and growth are both energetically favorable is called a critical nucleus.

Nucleation theory [37, 38] predicts that the rate of nucleation is limited by the concentration of the most stable critical nucleus, $[A_c]$. Intuitively, because more unfavorable reactions are required to form critical nuclei in a wider zig-zag tile set, $[A_c]$ should decrease exponentially with k. This argument is not rigorous, however, because unfortunately there are many more kinds of critical nuclei for larger values of k. The rate of spurious nucleation is proportional to the sum of the concentrations of all these critical nuclei. We will show in the following sections that despite this issue, under many conditions nucleation rates do decrease exponentially with k.

III. THE SELF-ASSEMBLY MODEL

To analyze the process of tile assembly, we formally describe the mass-action kinetic Tile Assembly Model (kTAM), which describes the composition of an assembly of tiles, the set of possible assembly reactions, and the dynamics of these reactions. While all aspects of the kTAM are not necessary to determine the rate of spurious nucleation with a zig-zag tile set, the kTAM has been previously used to analyze more complex tile programs [4, 5], and is a general framework for understanding algorithmic self-assembly.

A **tile type t** is a unit square, or a polyomino (a finite, connected set of unit squares) with bond types on each unit side of the tile. The set of possible **bond types** is referred to as Σ. A set of tile types is denoted by **T**. A tile (as contrasted with a tile type) is a tuple of a tile

type and a coordinate location $(x, y) \in \mathbb{Z}^2$. The set of tiles (all possible tile types in all possible locations) is referred to as T. Tiles cannot be rotated. Tiles that abut vertically or horizontally are **connected** if they have the same labels on the abutting sides. A set of tiles is connected if there is a path of connected tiles between any two tiles in the set.

An assembly A is an equivalence class with respect to translation of a non-overlapping, connected finite set of one or more tiles. The set of assemblies is denoted by $\mathcal{A}$. A set of tiles $\tilde{A}$ is considered the canonical representation of A if

$$\begin{aligned} \nexists \langle t, (x, y)\rangle \in \tilde{A} \text{ s.t. } & x < 0 \text{ or } y < 0 \\ & \text{and } \exists \langle t, (0, y)\rangle \in \tilde{A} \\ & \text{and } \exists \langle t, (x, 0)\rangle \in \tilde{A} \end{aligned}$$

That is to say, the canonical representation uses a coordinate system such that the assembly just fits in the upper right quadrant of the plane with no negative coordinates. $\tilde{A}(x, y)$ refers to the tile type at coordinates (x, y) in this representation, or 0 if there is no such tile. For an assembly A, $width(A) = \max_x |y_1 - y_2|$, such that $\langle \mathbf{t_1}, (x, y_1)\rangle, \langle \mathbf{t_2}, (x, y_2)\rangle \in A$. The length of A, $length(A)$, is defined analogously. The addition relation is defined between an assembly A and a tile t so that $A + t = B$ if and only if $\tilde{A}$ and t are connected but non-overlapping, and $\tilde{A} \cup t$ is a member of equivalence class B. For the attachment of two tiles to each other, we consider the set of tile types $\mathbf{T}$ to be listed in some order, and treat the first tile as an assembly. I.e., the addition relation is defined between two tiles t_1 and t_2, where t_1 comes before t_2. $t_1 + t_2 = A$ if and only if $t_1 = \langle t, (0, 0)\rangle$, t_1 and t_2 are connected but non-overlapping, and $t_1 \cup t_2$ is a member of equivalence class A. This definition is crafted to correctly count the number of distinct ways in which tiles can attach to each other. For example, two tiles of the same type with the same label on all four sides can attach in exactly four distinct ways.

If abutting labels on two connected tiles match, these tiles form a **bond**. The standard free energy, G°, of an assembly A is defined as $G^\circ(A) = -bG_{se}$, where b is the number of bonds in the assembly and G_{se} (the sticky end energy) is the free energy of a single bond.

The mass-action kTAM model considers reversible chemical reactions between tiles and assemblies occurring in well-mixed solution. In this paper, we consider all possible accretion reactions: reactions either between two tiles or between a tile and an assembly. We also assume that single tile concentrations are held constant during assembly (i.e. "powered"). In a powered accretion model of self-assembly, a reaction's rate is dependent on at most one changing concentration, so dynamics are linear. Early in crystallization, the period modeled here, most tiles are still unbound, and similarly most reactions are accretion reactions, so a powered accretion model is a reasonable approximation.

Formally, the set of **powered accretion reactions** are

$$\begin{aligned} R = \{ & A + t \to B + t,\ B \to A\ : \\ & A, B \in \mathcal{A} - T,\ t \in T,\ A + t = B\} \cup \\ & \{t_1 + t_2 \to A + t_1 + t_2,\ A \to \emptyset\ : \\ & t_1, t_2 \in T,\ A \in \mathcal{A} - T,\ t_1 + t_2 = A\} \end{aligned}$$

The appearance of single tiles on both sides of the association reactions and neither side of the dissociation reactions reflects the powered model's assumptions that the concentration of single tiles remains constant.

Mass-action dynamics and the powered accretion reactions define for each assembly a differential equation that describes the rate of change of the assembly's concentration in time. The concentration of assembly A is denoted by $[A]$. In general, for a chemical reaction $\sum_i n_i S_i \to \sum_j m_j S_j$ with rate constant k, where $n_i, m_j \in \mathbb{Z}^{\geq 0}$ and S_i are chemical species, mass-action dynamics [43] predict $\frac{d[S_j]}{ds} = k(m_j - n_j) \prod_i [S_i]^{n_i}$. These dynamics add linearly for multiple reactions.

In the kTAM, each reaction has a forward rate constant k_f that we assume to be the same for all reactions, and a backward rate constant $k_r = k_f e^{-\Delta G^\circ}$, where ΔG° is the difference between the sum of the standard free energies of the reactants and that of the products (where the standard free energy of a single tile is 0). The concentration of all tile types is held at $e^{-G_{mc}}$. (Identical concentrations are considered for convenience only; Appendix A shows how our formalism can be extended trivially to treat reactions where species have different concentrations.) Assemblies consisting of more than a single tile have an initial concentration of 0. Thus, for an assembly A at time point s,

$$\begin{aligned} \frac{d[A]}{ds} = k_f \Bigg(& \sum_{\substack{A+t \to B+t, \\ B \to A \in R}} e^{G^\circ(B) - G^\circ(A)}[B] - [A]e^{-G_{mc}} + \\ & \sum_{\substack{B+t \to A+t, \\ A \to B \in R}} [B]e^{-G_{mc}} - e^{G^\circ(A) - G^\circ(B)}[A] + \\ & \sum_{\substack{t_1+t_2 \to A+t_1+t_2, \\ A \to \emptyset \in R}} e^{-2G_{mc}} - e^{G^\circ(A)}[A] \Bigg). \end{aligned} \quad (1)$$

Each term in the first summation is the difference between the rate at which A and a tile react to form a larger assembly B and the rate at which the larger assembly B decomposes into A and a tile. Each term in the second summation is the difference between the rate of formation of A by a reaction where a single tile binds to a smaller assembly B, and the rate decomposition of A into assembly B and a single tile. The terms in the final summation are the rate of formation of A from two single tiles. In the remainder of this paper, we refer to

the mass-action kTAM with powered accretion reactions as simply "the kTAM".

The free energy $G(A)$, in contrast to the standard free energy, reflects both the entropy loss due to crystal formation and the enthalpy gain of assembly. It is defined as $G(A) = G^\circ(A) + \sum_{t \in A} G_{mc}$. The steady-state concentration of an assembly A is given by $[A]_{ss} = e^{-G(A)}$. For an assembly with n tiles and b bonds, this concentration is $[A]_{ss} = e^{(bG_{se} - nG_{mc})}$.

This model satisfies detailed balance within $\mathcal{A} - T$. That is, for all reaction pairs $A \to B$, and $A + t \to B + t$, $k_f[t][A]_{ss} = k_r[B]_{ss}$, where k_f and k_r are the forward and reverse rates in the respective reactions, and for reaction pairs $t_1 + t_2 \to A$ and $A \to \emptyset$, $k_f[t_1][t_2] = k_r[A]_{ss}$. For proof of this, see Appendix A.

IV. THERMODYNAMICS OF ZIG-ZAG ASSEMBLIES

To prove that nucleation rates of zig-zag ribbons decrease exponentially as their widths increase, we would first like to identify the critical nuclei for spurious nucleation. Thermodynamic constraints provide a powerful tool: by showing that undesirable assemblies have unfavorable energies, we can conclude that they occur rarely without having to consider rates. (In contrast, assemblies with favorable energies may or may not form quickly, depending upon details of the kinetics; such analyses form the bulk of Sections V and VI.)

We therefore consider the free energy landscape, where each point in the landscape corresponds to a particular type of assembly. Optimal control over nucleation is achieved in a regime where zig-zag growth is favorable, but the growth of less than full-width (thin) assemblies is unfavorable. The first condition is necessary for seeded assemblies to grow longer. The second condition restricts the possible pathways to spurious nucleation: long polymers cannot be created except by first growing to full width. This helps ensure that the bottleneck to spurious nucleation is a low concentration full-width assembly.

Within the kTAM, the energy landscape for assemblies is formally described by the free energy $G(A) = bG_{se} - nG_{mc}$, which can be evaluated directly for any given assembly A. G_{se} and G_{mc} describe the physical conditions for assembly. Changing G_{se} and G_{mc} can bring the system into two qualitatively different phases: in the melted phase, $G(A)$ is bounded below by $-G_{mc}$ for all A, meaning that no assembly has an appreciable concentration at steady state. In contrast, in the crystalline phase, $G(A)$ can continue to decrease without bound as certain polymeric assemblies become longer and longer – that is, adding a repeat unit to the assembly strictly decreases its free energy [50]. Within the crystalline phase, there are regimes where different types of long polymers are favorable or unfavorable, depending on the physical parameters. To ensure that thin polymers do not tend to grow, it is enough to show that for each of these polymer types, longer polymers have a more positive free energy than shorter ones.

To characterize the energy landscape formally, we consider the important classes of polymeric assemblies and evaluate their free energies. Figure 9(b), **B**-**F** show the 6 main types of polymeric assemblies [51] for ribbons of width 4 by indicating the repeat group that may be added (by a series of accretion reactions, as shown in Figure 10) to extend the polymer. To determine whether adding a repeat group results in a higher or lower energy assembly, we evaluate $\Delta G = G(A_{m+1}) - G(A_m) = \Delta n G_{mc} - \Delta b G_{se}$ where A_m is a polymeric assembly with m repeat units. If ΔG is negative, then longer polymeric assemblies of this type are more favorable and we can expect this kind of assembly to grow at some rate. This gives a linear condition on G_{se} and G_{mc}, specifying a regime of physical conditions in which a certain class of long assembly is favorable. For example, for polymer type **E**, each repeat unit adds 4 tiles ($\Delta n = 4$) and 6 bonds ($\Delta b = 6$) , so these polymers grow if $4G_{mc} - 6G_{se} < 0$, i.e. $\frac{G_{mc}}{G_{se}} < \frac{3}{2}$. Similar calculations result in the phase diagram shown in Figure 9(a), which shows the melted phase **A**, in which no polymers are favorable, and the crystalline phase divided into regimes **B**-**F** wherein one additional type of polymer becomes favorable in each successive regime. In all these calculations, the ratio $\tau \stackrel{def}{=} \frac{G_{mc}}{G_{se}}$ plays a critical role.

Figure 9(c) shows the $2k - 3$ classes of polymeric assemblies for the width k zig-zag tile set (excluding the full width ribbons) along with the condition on τ that governs when long polymers are favorable. When $2 > \tau > 2 - \frac{1}{2k-3}$, zig-zag growth is favorable, but long thin assemblies are less favorable than shorter ones.

Figure 11 illustrates the kinds of assemblies for which growing wider (rather than longer) is favorable. Very long assemblies can favorably grow wider even when τ is close to 2, so for optimal nucleation control it is necessary that lengthening of thin assemblies be unfavorable. Otherwise, a favorable path to nucleation exists: an assembly can grow until it is favorable for it to grow wider and then grow to full width.

An example of the difference in the energy landscape between the regime where only full width polymers are favorable ($2 < \tau < 2 - \frac{1}{2k-3}$), and a regime where other polymers are favorable can be seen in Figure 12. When $2 < \tau < 2 - \frac{1}{2k-3}$, as in the two left landscapes in this figure, the critical nuclei (denoted by the larger circles) are of width $k-1$ (or width k) for the two widths shown. The critical nuclei for the tile set of width 8 are more unfavorable than those of width 4. In contrast, when τ is outside this regime, as in the two right landscapes, a wider zig-zag tile set does not change the critical nucleus size and should not cause an exponential decrease in spurious nucleation rates.

Thus, the regime for optimal control over nucleation is limited to $2 > \tau > 2 - \frac{1}{2k-3}$. The primary theorem of the next section will be relevant only in this region. While the desirable region in the phase diagram appears small,

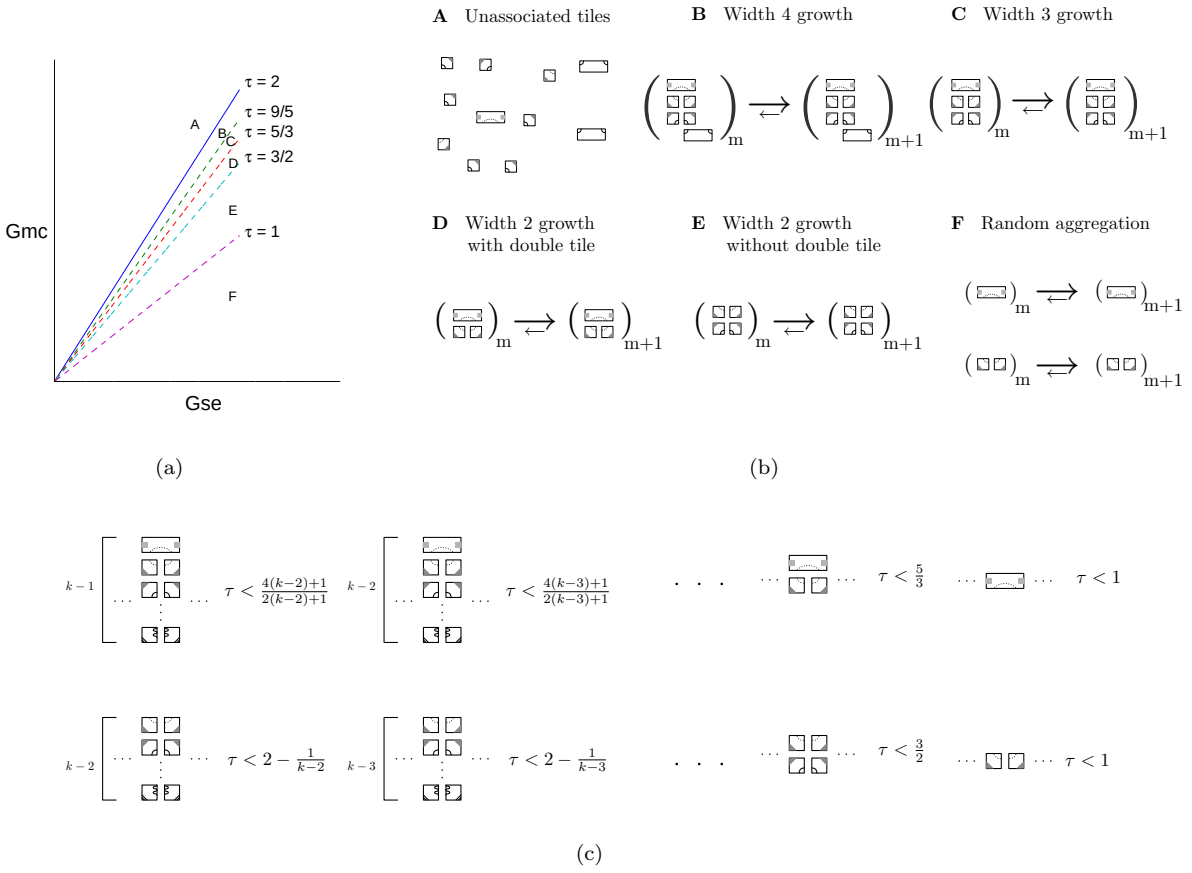

FIG. 9: **Physical conditions where zig-zag polymer elongation is favorable.** G_{mc} (ln(tile concentration)) and G_{se} (bond strength) define a set of physical conditions for zig-zag tile assembly. $\tau = \frac{G_{mc}}{G_{se}}$. **(a)** Phase diagram of the width 4 zig-zag tile set. In phase **A**, above the line $\tau = 2$, no assembly reactions are favorable, whereas in regimes **B**,**C**,**D**,**E** and **F**, progressively more types of assemblies (shown in (b)) become favorable. **(b)** The polymeric assemblies which become favorable in the regimes **B**-**F** shown in (a). A polymer is favorable when the energy change ΔG for adding a repeat unit becomes negative. If adding a repeat units adds n tiles and creates b new bonds, $\Delta G = nG_{mc} - bG_{se}$. For the polymer shown for regime **C**, for example, $\Delta G = 5G_{mc} - 9G_{se}$, which is negative when $\tau = \frac{G_{mc}}{G_{se}} < \frac{9}{5}$. Polymers shown for earlier regimes are also favorable in later phases: the polymer shown for regime **B** is favorable in regimes **C**-**F** and so on. **(c)** The assemblies that can form from a zig-zag tile set of width k and the physical conditions (in terms of τ) in which these assemblies becomes favorable. For a zig-zag tile set of width k, only full-width ribbons are favorable when $2 < \tau < \frac{4(k-2)+1}{2(k-2)+1} = 2 - \frac{1}{2k-3}$.

a slow anneal from a high temperature where $\tau \gg 2$ to a temperature in which $\tau < 1$ will pass through this regime, and a slow enough anneal will allow the bulk of the reaction to take place in this regime. Therefore, it is reasonable to consider a mechanism for the control of nucleation which is valid only in this narrow range of physical conditions. In the next section, we analyze the nucleation rates of the zig-zag tile set within this regime.

V. AN ASYMPTOTIC BOUND ON SPURIOUS NUCLEATION RATES

The kinetic Tile Assembly Model predicts the concentration of each assembly at all times. For most tile sets, the number of possible assemblies is large, and the individual concentrations of many kinds of intermediate assemblies are not necessarily of interest. Instead, it is often helpful to talk about the concentration of a **class** $\mathcal{C} \subset \mathcal{A}$ of assemblies, $[\mathcal{C}] = \sum_{A \in \mathcal{C}} [A]$.

The derivative of the concentration of a class of assemblies, $\frac{d[\mathcal{C}]}{ds} = \sum_{A \in \mathcal{C}} \frac{d[A]}{ds}$, can be calculated as the difference between the rate at which at which assemblies join the class and that at which they leave the class. Re-

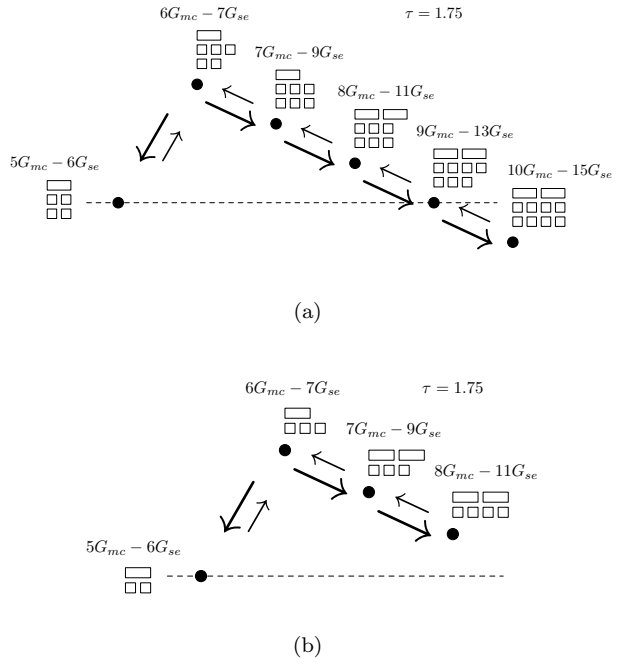

FIG. 10: **Zig-zag polymerization reactions.** The addition of a polymer unit to a thin assembly consists of an initial unfavorable accretion reaction followed by a series of favorable accretion reactions. **(a)** A favorable polymerization reaction. The positive free energy change from the four favorable accretion reactions is larger than the negative energy change from the initial unfavorable accretion reaction. Thus, polymers of width 3 are favorable where $\tau = 1.75$. **(b)** An unfavorable polymerization reaction. The positive free energy change from the two favorable accretion reactions is not large enough to compensate for the negative energy change from the initial unfavorable accretion reaction, so that polymers of width 2 are unfavorable where $\tau = 1.75$.

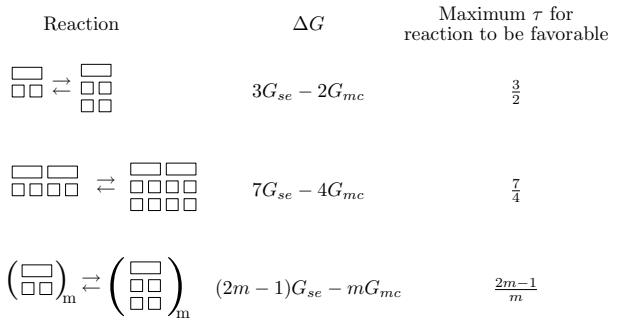

FIG. 11: τ **determines whether wider assemblies of a particular length are more favorable.** Like the polymerization of thin ribbons, a reaction to produce a wider assembly from a thinner one consists of an initial unfavorable accretion reaction followed by a series of favorable accretion reactions to complete the new row. The number of favorable reactions determines whether the overall reaction is favorable.

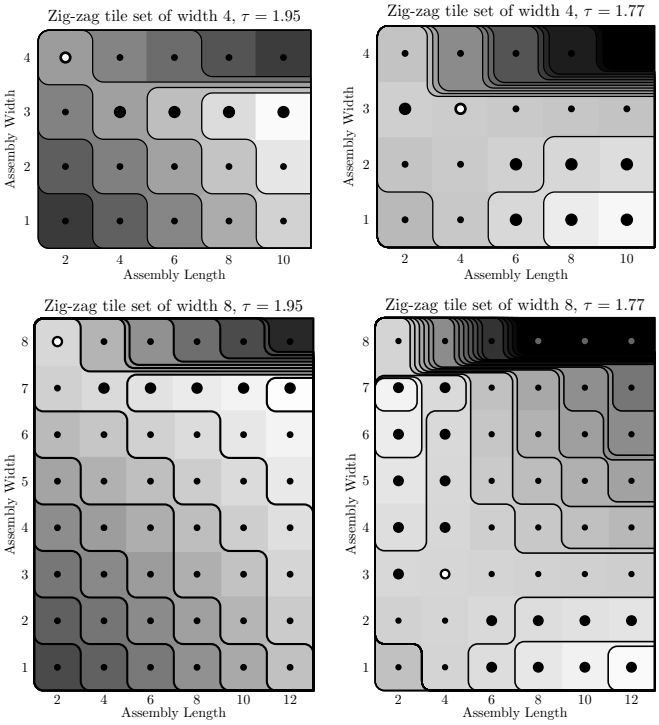

FIG. 12: **Example energy landscapes.** Coarse-grained depictions of the energy landscapes for two zig-zag tile sets of different widths under two different physical conditions. Each assembly is denoted by a circle. The shading in the square corresponding to each width and length represents the energy of a rectangular assembly of those dimensions. Darker is more favorable. Contour lines group assemblies of similar energies. Larger circles denote assemblies that are critical nuclei – those assemblies that can, through a series of favorable increases in length or width, reach full width. The most favorable critical nucleus, (the principal critical nucleus) is denoted by a large hollow circle. When $\tau = 1.95$, $2 < \tau < 2 - \frac{1}{2k-3}$ for both $k = 4$ and $k = 8$, so the critical nuclei are of width $k-1$ or k. Under these conditions, the most favorable path to nucleation for both tile sets is for a crystal of length 2 to grow to full width. Thus, the barrier to nucleation for a tile set of width 8 is higher than the barrier to nucleation for a tile set of width 4. In contrast, when $\tau = 1.77$, the principal critical nucleus is the same for both tile sets: it is an assembly of width 3 and length 4. Under these conditions, the spurious nucleation rate will not be appreciably smaller with the wider zig-zag tile set.

actions which produce new members of the class from assemblies not in the class are the **inward perimeter reactions**, $R^{in} = \{A + t \to B + t,\ A \to B,\ t_1 + t_2 \to B + t_1 + t_2 : A \notin \mathcal{C},\ B \in \mathcal{C}\}$. Reactions which use up members of the class to produce assemblies not in the class (or single tiles) are the **outward perimeter reactions** $= R^{out} = \{B + t \to A + t,\ B \to A,\ B \to \emptyset :\ A \notin \mathcal{C},\ B \in \mathcal{C}\}$.

Define the **flux** across a set of reactions R at time s as

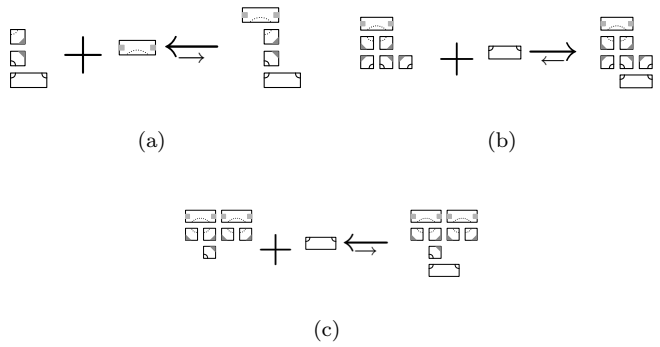

(a) (b) (c)

FIG. 13: **Spurious nucleation reactions.** Three spurious nucleation reactions for a zig-zag tile set of width 4. The reaction may be either favorable or unfavorable . In (b), the addition is favorable when $G_{mc} \approx 2G_{se}$, because two new bonds are formed; in (a) and (c), the addition is unfavorable, because in each reaction only one new bond is formed.

$$F(R,s) = \sum_{A+t\to B+t\in R} k_f[A]e^{-G_{mc}} + \sum_{B\to A\in R} k_f e^{G^\circ(B)-G^\circ(A)}[B] + \sum_{t_1+t_2\to A+t_1+t_2\in R} k_f e^{-2G_{mc}} + \sum_{A\to\emptyset\in R} k_f e^{G^\circ(A)}[A] \quad (2)$$

Then $\frac{d[\mathcal{C}]}{ds}(s) = F(R^{in},s) - F(R^{out},s)$.

We will use these formalisms to bound the rate of spurious nucleation in a zig-zag tile set of width k. The **spuriously nucleated assemblies** of width k will be denoted $\mathcal{C}_k$. Let the top tile in Figure 5(a) be designated $\mathbf{t_t}$ and the bottom tile be $\mathbf{t_b}$. Formally,

$$\mathcal{C}_k = \{A\in\mathcal{A} :\ \exists (x,y),(w,z)\in\mathbb{Z}^2 \text{ s.t. } A(x,y)=\mathbf{t_t}, A(w,z)=\mathbf{t_b},\ \}. \quad (3)$$

Note that the assemblies in $\mathcal{C}_k$ do not contain a seed tile, and we are measuring the rate of their formation in the absence of seed tiles.

The inward perimeter reactions for $[\mathcal{C}_k]$, which we call the **spurious nucleation reactions** and denote by R_k^{in}, are the reactions for which the product is a full width assembly, but the reactant is not. In other words, they are the addition reactions which produce width k assemblies from assemblies of width $k-1$ by adding either or a top or bottom double tile (Figure 13). As shown in Section IV, when $2 < \frac{G_{mc}}{G_{se}} < \frac{1}{2k-3}$, these reactions demarcate the point at which sustained growth can proceed by exclusively favorable steps. The outward perimeter reactions, which we call the **ribbon shrinking reactions** and denote by R_k^{out}, are those in which a tile falls off a full width assembly to produce an assembly of width $k-1$. For assemblies that have suffered a ribbon shrinking reaction, there is now a downhill path to complete melting in the energy landscape of the type shown in Fig. 12, when $2 < \frac{G_{mc}}{G_{se}} < \frac{1}{2k-3}$.

The overall rate of spurious nucleation of width k zig-zag crystals (in units of Molar per second),

$$n_k(s) = \frac{d[\mathcal{C}_k]}{ds}(s) = F(R_k^{in},s) - F(R_k^{out},s),$$

may be integrated over time to obtain the total concentration of spuriously nucleated assemblies. Furthermore, an upper bound on $n_k(s)$ similarly translates into an upper bound on the concentration of spuriously nucleated assemblies. Because the growth path for full-width ribbons is so favorable (zig-zag growth), one such bound is obtained by neglecting the ribbon shrinking reactions reactions and considering just the spurious nucleation reactions:

$$n_k^+(s) = F(R_k^{in},s) > n_k(s).$$

In the following, we use the phrase "the rate of spurious nucleation" to refer to the overall rate at which the concentration of spuriously nucleated assemblies increases, $n_k(s)$, whereas the phrase "the rate of spurious nucleation reactions (or events)" refers to the rate of tile additions that create full-width ribbons from less-than full-width assemblies regardless of whether or not those assemblies subsequently shrink again, i.e., $n_k^+(s)$.

Theorem 1. *For a zig-zag tile set of width $k > 2$, if $2 > \frac{G_{mc}}{G_{se}} > 2-\delta$, $\delta < \frac{1}{2k-3}$, and $G_{se} > \frac{2k\ln 2}{1-(2k-3)\delta}$, then for all times s, $n_k(s) < 4k_f e^{(\delta-k)G_{se}}$.*

Proof. All the spurious nucleation reactions are addition reactions, so the second and fourth terms of the flux expression in Equation 2 are both zero. Spuriously nucleated assemblies are defined as assemblies of width k, so the reactants in the spurious nucleation reactions are of width $k-1$ (only accretion reactions are allowed). For a tile set of width $k > 2$, the third term of Equation 2 – the contribution of the interaction of two tiles – also drops out. Therefore, for a tile set of width $k > 2$ with spurious nucleation reactions R_k^{in},

$$n_k(s) \le n_k^+(s) = \sum_{A+t\to B+t\in R_k^{in}} k_f[A]e^{-G_{mc}}, \quad (4)$$

where $[A]$ is the concentration of assembly A at time s.

The following lemma shows that the concentration of an assembly can be bounded by its concentration at steady state [52]:

Lemma 1. *In a mass-action powered accretion model of self-assembly that has an initial state containing only*

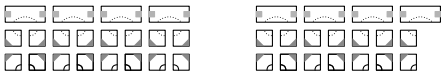

(a) (b)

FIG. 14: **Assembly dimensions of rectangular assemblies.** **(a)** A $k-1=3$ by $l=8$ assembly. **(b)** A $k-1=3$ by $l=7$ assembly.

single tiles, every assembly has a concentration less than or equal to its steady state concentration.

Proof. See Appendix B. □

Lemma 1 implies that

$$F(R_k^{in}, s) \leq \sum_{A+t \to B+t \in R_k^{in}} k_f [A]_{ss} e^{-G_{mc}}.$$

where $[A]_{ss}$ is the concentration of assembly A at steady state.

Partitioning the summation according to the length of the reactant assembly gives

$$F(R_k^{in}, s) \leq \sum_{l=1}^{\infty} \sum_{\substack{length(A)=l \\ A+t \to B+t \in R_k^{in}}} k_f [A]_{ss} e^{-G_{mc}}. \quad (5)$$

To be a reactant in a spurious nucleation reaction, A must have a width of $k-1$. By assumption, A cannot have any mismatches [53]. Thus, each assembly A in the preceding summation can be viewed as a $k-1$ by l rectangular assembly of the type shown in Figure 14 with zero or more tiles missing [54]. $2G_{se} > G_{mc}$, so the free energy of a $k-1$ by l assembly cannot be more favorable than the free energy of the $k-1$ by l rectangle that contains it, since any missing tiles in the rectangle could be added by favorable reactions. Therefore, the concentration of any $k-1$ by l assembly at steady state must be no larger than the concentration of its corresponding $k-1$ by l rectangular assembly. Note that this bound is very loose, since most assembly types have several tiles attached by only one bond. Let $A_{k-1,l}$ be a $k-1$ by l rectangular assembly, and $C(k-1,l)$ be the number of assemblies of width $k-1$ and length l. Each assembly can bind a single tile in up to l locations along either the top or bottom edge. Thus,

$$\begin{aligned} F(R_k^{in}, s) &< \sum_{l=1}^{\infty} \sum_{\substack{length(A)=l \\ A+t \to B+t \in R_k^{in}}} k_f [A_{k-1,l}]_{ss} e^{-G_{mc}} \\ &\leq \sum_{l=1}^{\infty} C(k-1,l) l k_f [A_{k-1,l}]_{ss} e^{-G_{mc}}. \end{aligned}$$

A counting argument shows that $C(k-1,l) < 2^{(k-1)l+1}$, so

$$F(R_k^{in}, s) < 2 \sum_{l=1}^{\infty} 2^{(k-1)l} l k_f [A_{k-1,l}]_{ss} e^{-G_{mc}}.$$

The steady state concentration of an unseeded assembly with n tiles and b bonds is given by $[A]_{ss} = e^{-nG_{mc}+bG_{se}}$. The assembly $A_{k-1,l}$ contains $(k-2)l$ small tiles and $\lceil l/2 \rceil$ top (or bottom) tiles. There are $(l-1)(k-2)$ horizontal bonds between small tiles and $\lceil l/2 \rceil - 1$ horizontal bonds between large tiles. In addition, there are up to l vertical bonds in each of the $k-2$ spaces between rows of tiles. Therefore,

$$\begin{aligned} [A_{k-1,l}]_{ss} \leq \exp\big[&- \left((k-2)l + l/2\right) G_{mc} + \\ &\left((k-2)(l-1) + l/2 + (k-2)l\right) G_{se} \big]. \end{aligned}$$

Applying the assumption $G_{mc} > (2-\delta)G_{se}$ and simplifying,

$$[A_{k-1,l}]_{ss} < \exp\left[(2-k)G_{se} + (k\delta - \frac{1}{2} - \frac{3\delta}{2}) l G_{se} \right].$$

Thus,

$$\begin{aligned} F(R_k^{in}, s) < 2k_f e^{-G_{mc}} e^{(2-k)G_{se}} \\ \sum_{l=1}^{\infty} 2^{(k-1)l} e^{(k\delta - \frac{1}{2} - \frac{3\delta}{2}) l G_{se}} \end{aligned}$$

Since $k\delta - \frac{1}{2} - \frac{3\delta}{2} < 0$ when $\delta < \frac{1}{2k-3}$, bounding G_{se} from below preserves the inequality. Therefore, when $G_{se} > \frac{2k\ln(2)}{1-(2k-3)\delta}$,

$$\begin{aligned} F(R_k^{in}, s) &< 2k_f e^{-G_{mc}} e^{(2-k)G_{se}} \\ &\qquad \sum_{l=1}^{\infty} l 2^{(k-1)l} e^{(k\delta - \frac{1}{2} - \frac{3\delta}{2}) l \frac{2k\ln(2)}{1-(2k-3)\delta}} \\ &= 2k_f e^{-G_{mc}} e^{(2-k)G_{se}} \sum_{l=1}^{\infty} l 2^{(k-1)l} e^{-kl\ln 2} \\ &= 2k_f e^{-G_{mc}} e^{(2-k)G_{se}} \sum_{l=1}^{\infty} l 2^{-l} \\ &= 4k_f e^{-G_{mc}} e^{(2-k)G_{se}} \\ &= 4k_f e^{(\delta-k)G_{se}} \end{aligned}$$

□

This theorem says that the spurious nucleation rate, n_k, decreases exponentially with k and with G_{se}, within the limits of applicability of the theorem – which requires larger G_{mc} for larger k, and hence slower growth rates. The strength of the theorem, therefore, lies in the extent to which spurious nucleation decreases *faster* than the

growth rate, r_k, of seeded crystals. These relative rates translate into the degree of purity that can be obtained when attempting to grow seeded crystals: suppose the concentration of seeds is c, and they are grown to a length L during a time period $s = L/r_k$. The concentration of unseeded crystals that will have spuriously nucleated in that time is $s \cdot n_k = L \cdot \frac{n_k}{r_k}$, i.e., the fraction of crystals that were spuriously nucleated is $\frac{L}{c} \cdot \frac{n_k}{r_k}$. (When we use n_k without specifying a particular time, we mean the asymptotic value, which is an upper bound.) Regardless of what length or amount of seeded crystals is desired, reducing $\frac{n_k}{r_k}$ is the relevant metric for increasing the yield of desired structures.

One way to study the trade-off between n_k and r_k is to ask, given a target growth rate r, what is the lowest nucleation rate that can be achieved by adjusting G_{mc} and G_{se} while maintaining $r_k = r$? Previous work [19] has shown that near the $\tau = 2$ phase boundary that is relevant to our theorem, the growth rate is closely approximated by, and for the purposes of this paper defined as,

$$r_k = \frac{k_f}{k-1}(e^{-G_{mc}} - e^{-2G_{se}}),$$

measured in layers per second. The lowest nucleation rate for a given target growth rate r is then

$$n_k^*(r) = \min_{G_{se},G_{mc} \text{ s.t. } r_k=r} n_k.$$

A plot of $n_k^*(r)$ vs r, if it could be calculated, would reveal how much the spurious nucleation rate can be decreased for a given decrease in the growth rate, for zig-zag crystals of a given width. Theorem 1 only gives us an upper bound on $n_k^*(r)$, but even so, this already gives us a characterization of the advantage provided by wider zig-zag crystals.

Specifically, choosing $2G_{se} - G_{mc} = \epsilon = \ln k$ and $\delta = \frac{1}{2}\frac{1}{2k-3}$ and $G_{se} > 4k \ln k$, Theorem 1 guarantees that $n_k^* < n_k < 4ek_f e^{-kG_{se}} \stackrel{def}{=} n_k^1$, while $r_k = \frac{k_f}{k-1}(e^{\epsilon-2G_{se}} - e^{-2G_{se}}) = k_f e^{-2G_{se}}$. The bound n_k^1 is plotted against r_k in Fig. 15 using log-log axes; the slope $(\frac{k}{2})$ indicates that the spurious nucleation rate decreases polynomially with the growth rate, and the polynomial degree increases with wider zig-zag tile sets. Thus, for $k > 2$, spurious nucleation does decrease faster than the growth rate. While these bounds characterizing the tradeoff between n_k^* and r_k are rigorous, because Theorem 1 is so loose, it is expected that n_k^* is actually much lower than the bound n_k^1. In the following sections, we will see that this is true; furthermore, the true slopes are even steeper than obtained here.

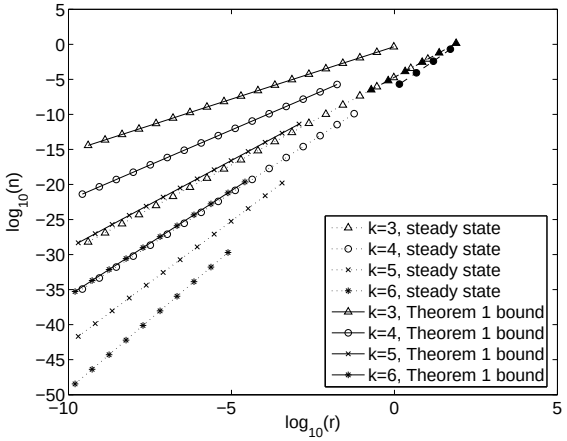

FIG. 15: **Calculated steady state nucleation rates**. Asymptotic bounds given by Theorem 1 and numerical calculations of nucleation rates at steady state as described in Section VI A. The graph compares the growth rate r_k (in layers / s) and the rate of spurious nucleation events, n_k^+ (in M / s), for $\epsilon = 0.1$. Since the forward rate constant k_f has not been measured experimentally for tile-based assembly, we use $k_f = 6 \times 10^5$/M/s based on typical oligonucleotide hybridization rates [44]. Filled triangles and circles denote rates of spurious nucleation events for $k = 3$ and $k = 4$ respectively, estimated from stochastic simulations, and are plotted in more detail in Figure 16. They are plotted here to illustrate that these measured rates are consistent with the calculated rate of steady state spurious nucleation.

VI. NUMERICAL ESTIMATES OF SPURIOUS NUCLEATION RATES

Having shown in the previous section that zig-zag tile sets can be designed to achieve arbitrarily low spurious nucleation rates relative to the growth rates, we now ask whether the nucleation barrier provided by zig-zag tile sets is sufficient for practical implementation in the laboratory. There are two main concerns: first, as each tile must be synthesized, k must be small (6 is currently practical, while 50 is currently too large); second, assembly time must not be too long (growing 1000 layers of seeded crystals with less than 1% spurious nucleation – which we refer to as the "typical reaction" – seems like a reasonable goal to accomplish within one week). As the asymptotic bounds of Section V are too loose for obtaining a realistic evaluation of nucleation rates for small k, we now develop more accurate numerical calculations and stochastic simulations for estimating spurious nucleation rates.

The analysis in Section V overestimates the spurious nucleation rate in three ways. First, it overestimates the concentration of almost all kinds of assemblies by assuming they have the same concentration as a rectangular assembly of the same length and width, and it overcounts the number of different types of assemblies.

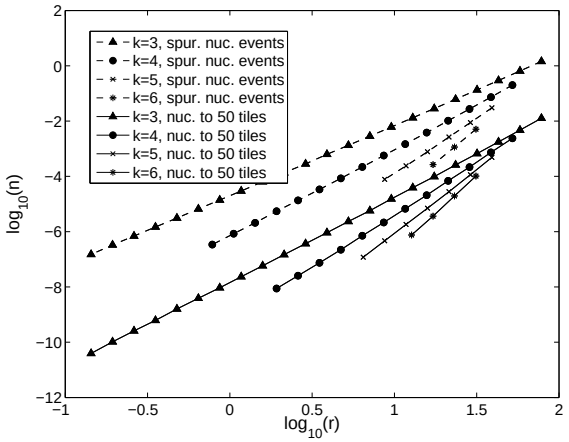

FIG. 16: **Estimates of nucleation rates from simulations.** Estimates of the ratio between assembly speed r_k and the average, over the time needed for seeded crystals to grow 1000 layers, of the rate of spurious nucleation events ($\frac{1}{s}\int_0^s n_k^+(s)$) or the overall spurious nucleation rate ($\frac{1}{s}\int_0^s n_k(s)$), as measured by stochastic simulations either (a) counting the frequency of reactions that create full-width ribbons, i.e., R_k^{in}, or (b) counting the number of assemblies that have 50 tiles or more. $\epsilon = 0.1$. Simulations are only practical for high concentrations, and the numerical calculations of Fig. 15 are only provably valid for lower concentrations.

Second, Lemma 1 shows that the spurious nucleation rate at steady state is the maximal spurious nucleation rate. However, it may take longer to approach steady state than the time needed to run a "typical reaction". Lastly, this analysis defines a spurious nucleation event for a zig-zag tile set of width k as a reaction that produces an assembly of width k, and neglects the backward reaction. In practice, many reactions that form an assembly of width k are unfavorable, so that the product assembly frequently shrinks back to a sub-critical size instead of growing larger. Furthermore, when conditions only slightly favor growth, even assemblies containing several layers have a reasonable chance of shrinking to nothing before they grow substantially. I.e., we expect $n_k << n_k^+$.

In this section, we describe three numerical techniques that correct each inaccuracy for zig-zag tile sets of widths $k = 3, 4, 5$ and 6. In Section VI A, we much more accurately compute the rate at which ribbons of width k are formed at steady state. These computations show that the asymptotic bound of Theorem 1 is too high by at least 4 orders of magnitude for the range of parameters studied. In Section VI B we use a stochastic simulation of tile assembly to estimate the rate of spurious nucleation reactions R_k^{in}. Our results indicate that spurious nucleation reactions occur during a "typical reaction" at virtually the same rate as at steady state. In Section VI C, we use the stochastic simulation to investigate whether the rate of spurious nucleation reactions ($n_k^+ = F(R_k^{in}, s)$) in a typical reaction accurately predicts the rate at which large assemblies appear (which at steady state is equivalent to $n_k(s) = F(R_k^{in}, s) - F(R^{out}, s)$). We find that for the range of parameters studied, at least 99% of assemblies that reach full width will melt before growing into large crystals, and thus our other estimates of spurious nucleation rates may be overestimates of n_k by at least this factor. In Section VI D, we show that these results together indicate that a zig-zag tile set of width 5 or 6 should be large enough to prevent almost all spurious nucleation in a "typical reaction", while maintaining reasonable assembly speeds. We discuss an important caveat: our results are derived under a powered accretion model of kTAM, while in experiments, small assemblies may aggregate rather than growing exclusively by single tile additions, thus potentially producing nuclei that reach a critical size more quickly than our simulations indicate.

A. Spurious Nucleation Rates at Steady State

Recall that for a zig-zag tile set of width $k > 2$, the steady state rate of spurious nucleation reactions is given by the sum

$$n_k^+ = \lim_{s\to\infty} F(R_k^{in}, s) = \sum_{l=1}^{\infty} \sum_{\substack{A+t\to B+t\in R_k^{in} \\ \text{s.t. } length(A)=l}} k_f [A]_{ss} e^{-G_{mc}},$$

which ignores the rate at which spuriously nucleated assemblies dissolve back into pre-nucleated assemblies. While $[A]_{ss}$ is known (at steady state, for an assembly A with n tiles and b bonds, $[A]_{ss} = e^{bG_{se} - nG_{mc}}$), it is not practical to compute the sum exactly because there are an infinite number of spurious nucleation reactions. Additionally, it can be impractical to evaluate the inner sum even for a single value of l: no efficient algorithm is known (see e.g. [45] for the related problem of counting polyominos) for exactly enumerating the reactions in R_k^{in}. The number of distinct reactions increases exponentially with the length of A, so that it is prohibitive to calculate all but the first terms of the sum.

Despite these difficulties, the expression can be calculated precisely, with known error bounds, for many k. The following lemma shows that under many reaction conditions of interest, the sum converges quickly, so that its value can be approximated by summing only the first few terms:

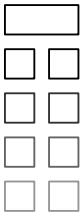

FIG. 17: **Hypothesized critical nucleus for most spurious nucleation reactions.** The rate of spurious nucleation reactions by this assembly (shown in different shades of gray for tile sets of widths 3,4,5,and 6) accounts for a large portion of spurious nucleation at slow speeds, and also accounts for the rate of increase in spurious nucleation rates as assembly gets faster.

Lemma 2. *When* $G_{se} > (\ln 10)(k-2) + \ln 4$, $G_{mc} = 2G_{se} - \epsilon$, $0 \leq \epsilon < \frac{1}{2k-3}$ *and* l *is even,*

$$\sum_{p=l+1}^{\infty} \left(\sum_{\substack{A+t \to B+t \in R_k^{in} \\ s.t.\ length(A)=p}} k_f [A]_{ss} e^{-G_{mc}} \right) < 2 \left(\sum_{\substack{A+t \to B+t \in R_k^{in} \\ s.t.\ length(A)=l}} k_f [A]_{ss} e^{-G_{mc}} \right)$$

Proof. See Appendix C. □

Thus, to calculate the spurious nucleation rate up an accuracy of $\frac{1}{\delta}$, it is only necessary to compute the inner sums of the series until the sum the current value of l is (even and) less than $\frac{1}{2\delta}$. (Note that this approach does not directly yield a proof of an asymptotic bound for arbitrary k, because the formula for the nucleation rate is not a closed form expression.)

We have used this series truncation method to calculate the rate of spurious nucleation to 2 parts in 10^5 for $k = 3, 4, 5, 6$ and for a range of G_{se}, G_{mc} for which $\epsilon = 0.1$. The values of G_{se}, G_{mc} and k used were in a regime in which Lemma 2 applies. The results are shown in Figure 15.

In addition to the numerical calculations providing lower estimates, the slopes of $\log n_k^+$ vs $\log r_k$ in Fig. 15 are larger than those of $\log n_k^1$ vs $\log r_k$. Specifically the numerical calculations give slopes $\frac{k+2}{2}$, compared to the asymptotic bounds that give slopes $\frac{k}{2}$. Is this reasonable? In the limit as $G_{mc} \to \infty$, all spurious nucleation should be dominated by the single species with the highest steady state concentration (adding tiles become so unfavorable that other species can be neglected.) The analysis in Section IV suggests that this assembly is the one shown in Figure 17. The steady state concentration of this assembly A for a tile set of width k is $[A]_{ss} = e^{-(2k-3)G_{mc}+(3k-6)G_{se}} = e^{-kG_{se}+(2k-3)\epsilon}$. If all forward nucleation reactions involve A, then

$$n_k^+ = 2k_f [A]_{ss} e^{-G_{mc}} = 2k_f e^{-(k+2)G_{se}+(2k-4)\epsilon}$$

while the speed of growth is

$$r_k = k_f e^{-2G_{se}} \frac{e^{\epsilon} - 1}{k-1},$$

and thus the slope would be $\frac{k+2}{2}$, as observed. Even for the range of smaller G_{mc} for which numerical calculations were performed, this estimate of n_k^+ is based on assuming a single critical species is within a factor of three of the precisely calculated value. These results echo the more general result achieved in Section V.

Tile set width	Steady state	Typical reaction	50 tile assemblies in a typical reaction
3	1e11 years	$< 9e10$ years	< 5000 years
4	40 years	< 40 years	< 30 days
5	10 days	< 20 days	< 10 hours
6	7 hours	< 20 hours	< 2 hours

TABLE I: **Time needed to grow 1000 layers such that less than 1 percent of assemblies are spuriously nucleated.**

B. Stochastic simulations for estimating forward nucleation rates before steady state is achieved

In order to determine whether steady state is a good approximation for what happens in a typical spurious nucleation reaction, we simulated zig-zag tile assembly for tile sets of widths $k = 3, 4, 5$ and 6 and measured the rates of spurious nucleation events during the time it should take to grow 1000 layers from seeds. Since there are an infinite number of powered accretion reactions, exact simulation of growth under the kTAM using mass action dynamics is not possible. Instead, we simulated assembly growth using stochastic chemical reaction dynamics. To approximate the nucleation rate, we simulate a tiny reaction volume, and use these results to predict the nucleation rate in a much larger volume.

We used the Gillespie algorithm [46] to sample the trajectories of stochastic dynamics of the zig-zag tiles in a small volume V, chosen to ensure accuracy as described below. Following the powered model, our simulation assumes the concentration of each tile type to be constant and explicitly tracks each assembly containing more than one tile. Initially, no multi-tile assemblies are present. Single tiles are present at a concentration of $e^{-G_{mc}}$ so that the rate of two tiles colliding (and thus producing a new assembly to be explicitly tracked) is $\mathbf{A} k_f V e^{-2G_{mc}}$

molecules / second. For each assembly containing two or more tiles, the rate of tile addition is $k_f e^{-G_{mc}}$ and the rate that a tile with b bonds falls off an assembly is $k_f e^{-bG_{se}}$.

For $k = 3, 4, 5, 6$ and a range of G_{se} and G_{mc} where $\epsilon = 0.1$, we counted the number of spurious nucleation events, m, that took place over the time course of a "typical reaction", $s = 1000/r_k$, in a volume V that was chosen large enough to ensure that statistical error in m is less than 10 percent of its value ($P > 0.95$). If our simulations yield a nucleation rate of m events per second, the molar rate of nucleation events for a bulk volume is given by $n_k^+ \approx \frac{m}{V\mathbf{A}}$ where $\mathbf{A}$ is Avogadro's number. The results of the simulation – which were possible only for small enough G_{se} such that nucleation events were frequent enough to be counted – are shown in Figure 16. For $k = 3$ and $k = 4$, these rates are within a factor of 2, and for all values tested, these rates are within a factor of 10 of the linear extrapolation of the curves from Fig. 15, indicating that the choice in Section V to bound nucleation rates based on steady-state concentrations did not affect our estimate of nucleation rates too greatly. This should be expected, given that most steady state nucleation appears to involve assemblies like the one shown in Figure 17.

C. Nucleation of Long Ribbons

In this paper, we have defined a spurious nucleation reaction for a zig-zag tile set of width k as a reaction in which an assembly of width $k-1$ grows to width k. The goal was that this definition would be inclusive, such that all long ribbons would undergo at least one spurious nucleation reaction, but not too loose, such that most spurious nucleation reactions lead to a long ribbon. However, many of these spurious nucleation reactions are not energetically favorable - an assembly may briefly reach width k before a tile falls off. The assembly then either melts or undergoes another spurious nucleation reaction.

At what rate do long ribbons appear? Using the stochastic simulation described in the last section and the same range of physical reaction parameters, we measured m', the number of ribbons containing 50 tiles or more that were present at the end of a "typical reaction", for the widths 3,4,5, or 6. This counts the number of spurious nucleation events that did *not* subsequently melt, and thus it provides the basis for an estimate for n_k. As only those crystals that nucleated sufficiently far before the end of the simulation will have grown to a large enough size to have been counted, so we use the formula $n_k \approx \frac{m'}{(s-50/(k-1)/r_k)V\mathbf{A}}$. The results are shown in Figure 16.

While the assumption that concentrations of unnucleated assemblies had reached steady-state appears to have been inconsequential, these simulations indicate that the assumption that a spurious nucleation reaction always produces a long ribbon did cause a significant overestimate of the amount of spurious nucleation. They suggest that most (at least 99%) of assemblies that reach critical size will subsequently melt.

D. Expected effectiveness in practice

Do these results indicate that nucleation control with tile sets of width 6 or less are good enough? Recall that our "reasonable goal for a typical reaction" addresses how much time is needed to grow seeded ribbons of 1000 layers with less than 1% of the crystals being spuriously nucleated. The fraction of crystals that are spuriously nucleated is given by $f = \frac{L}{c}\frac{n_k}{r_k}$ where L is the number of layers to be grown on seeds, and c is the concentration of seeds. While the simulations only measured n_k for large values of r_k, it is possible to bound n_k from above for smaller values of r_k by linearly extrapolating the lines in Figure 16, because the slopes $\log n_k$ vs $\log r_k$ should be no smaller than at steady state, $\frac{k+2}{2}$. Taking $c = \frac{1}{L}e^{-G_{mc}}$, we use this technique to bound r_k from above, and therefore to bound the time necessary to grow 1000 layers on average where less than 1% of the crystals are spuriously nucleated. The results, shown in Table I, are encouraging. They suggest that, using a zig-zag tile set of width 6, just a few hours would be enough to avoid most spurious nucleation.

The analysis and simulations in this section support the idea that nucleation control using the zig-zag tile set not only works, but is practical. While in most respects our models appear complete, two effects which may be important in the actual process of assembly are not included. One important effect is tile depletion: while our model considers the concentration of free tiles to be constant, in a typical experiment tiles are used up because they join assemblies. Since the rate of spurious nucleation is concentration dependent, we would expect the rate of spurious nucleation to be larger at the beginning of a reaction, when almost all free tiles remain, than at the end, when many tiles are used up. Because of this effect, our simulations may actually *overestimate* the spurious nucleation rate.

However, our simulations also neglect an important possible reaction pathway that may greatly increase the rate of spurious nucleation. While our model assumes tiles must be added to assemblies one at a time, in an experiment, small assemblies can also attach to each other. The formation and joining of several small assemblies may be faster than the spurious nucleation pathways described in this paper. A complete understanding of spurious nucleation of zig-zag tiles requires an understanding of the speed of spurious nucleation reactions caused by aggregation.

VII. CONCLUSIONS

A. Nucleation of Algorithmic Self-Assembly

Our original motivation for this work was to show that self-assembly programs that work in the aTAM, in which it is straightforward to design tile sets that algorithmically assemble any computationally defined structure, can also be made to work in the more realistic kTAM. Tiles sets that assemble correctly via unseeded growth in the aTAM with a threshold of $\tau = 1$ will assemble correctly in the kTAM under the right conditions. However, tile sets that are designed to assemble via seeded growth in the aTAM with a threshold $\tau = 2$ may fail in the kTAM because mismatch, facet and spurious nucleation errors occur. These problems are ameliorated in the limit of slow assembly speed [19]. Other work has described methods to control mismatch errors and facet errors without significant slowdown [26, 27, 28]. Here, we have developed a construction that corrects the last discrepancy, spurious nucleation errors, again without significant slowdown.

However, it remains to be formally proven that these constructions can be combined to control all types of errors simultaneously for any tile set of interest. No major difficulties are expected, in large part because mismatch and facet errors can both be controlled by a single mechanism [27] and the control of spurious nucleation errors works independently of this mechanism. Both methods work by transforming an original tile set which works in the aTAM at $\tau = 2$ into a new (typically larger) tile set that is more robust to particular kinds of errors in the kTAM. Additionally, the combination of these error correction mechanisms is expected to be experimentally tractable: the cost of both these transformations is a moderate increase in spatial scale and the number of tile types.

We expect that the zig-zag tiles can be used as a subroutine in more complex algorithmic self-assembly programs when control of nucleation is needed. Other self-assembly programs for controlling nucleation are certainly possible; we do not know whether the zig-zag tile sets are optimal.

B. Detection of a Single DNA Molecule

Control over nucleation in algorithmic self-assembly can be seen as a special case the detection of a single molecule. For a tile set of sufficiently large width, essentially nothing happens when no seed tiles are present, whereas if even a *single* seed tile is added, growth by self-assembly will result in a macroscopic assembly. Theorem 1 shows that the *false-positive* rate for detection can be made arbitrarily small by design; the *false-negative* rate in the kTAM is approximately 0. Although this idealized model does not consider many factors that could lead to poorer detection in a real system, we don't know of any insurmountable problems with implementing single-molecule detection this way.

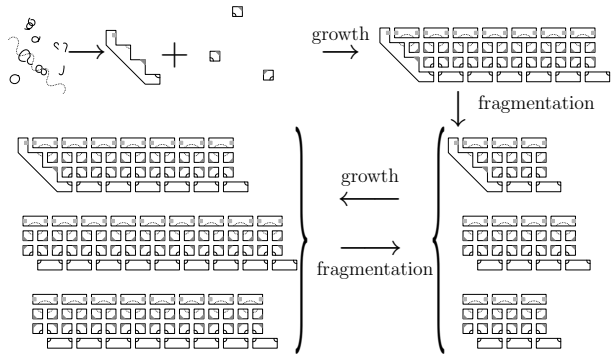

FIG. 18: **Exponential amplification of assemblies.** Probe strands assemble onto a target sequence to create a seed assembly, which nucleates zig-zag growth. Periodic fluid shear causes fragmentation of zig-zag assemblies, leading to exponential amplification. The diagonal structure of the seed assembly shown here is a natural shape for assembling tiles on a scaffold strand [15].

There are, however, two immediate drawbacks. First, detecting seed-tile assemblies is not as useful as detecting arbitrary DNA sequences. Second, the linear growth of a single zig-zag assembly would require a long time lapse before a macroscopic change is perceptible. As sketched in Figure 18, we can surmount both obstacles. First, as in [14, 47], a set of strands can be designed to assemble double-crossover molecules on a (sufficiently long) target strand with nearly arbitrary sequence, thus creating the seed assembly if and only if the target strand exists. Second, since fluid shear forces can fragment large DNA assemblies, intermittent pipetting or vortexing will break large zig-zag assemblies, increasing the number of growing ends with each fragmentation episode. This fragmentation process can be expected to lead to exponential growth in the number of zig-zag assemblies without increasing the false-positive rate. (When a spuriously nucleated assembly does eventually form, of course, it will also be exponentially amplified.)

Based on the analyses of the previous section, we can estimate the effectiveness of this procedure. Is there a reasonable tile set width for which a single seed could amplify to a level of detectability in a reasonably short time without any spurious nucleation occurring within the given volume? Specifically, given a 10 μL reaction volume, a minimum detection level of 10^5 crystals and a protocol in which assemblies split after growing on average to size 200 layers, we would like to determine the minimum time and tile set width that meets these requirements. Creating 10^5 crystals requires first growing from the seed to size 200, then 17 cycles of fragmentation followed by growing 100 additional layers (50 on each side), so amplification requires $t_a = 850/r_k$ seconds. The expected time for the first nucleation event is $t_f = \frac{1}{n_k V \mathcal{A}}$, and our criteria for reliable detection is $t_f > 100 t_a$, i.e.

$\frac{n_k}{r_k} < \frac{1}{85000V\mathcal{A}}$. Based on Figure 16, we use the approximation $\log(n_k) + 2 = \frac{k+2}{2}(\log(r_k) - 1.7)$. Solving for t_a as a function of k, we find that good results are obtained for experimentally feasible widths. For example, with $k = 12$, reliable detection of a single seed in $V = 10$ μL is $t_a \approx 26$ hours.

VIII. ACKNOWLEDGEMENTS

The authors are grateful to Ho-Lin Chen, Ashish Goel, Zhen-Gang Wang and Deborah Fygenson for helpful advice and discussions and to Donald Cohen for advice on extending the results included here. This work was supported by NSF CAREER Grant No. 0093486 to EW, NASA grant NNG06GA50G to EW, and an NSF Graduate Fellowship to RS. An extended abstract of this work appeared previously as "Programmable Control of Nucleation for Algorithmic Self-Assembly" in the Proceedings of the 10th International Workshop on DNA Computing.

APPENDIX A: MASS-ACTION KTAM SATISFIES DETAILED BALANCE

This section contains proof that the mass-action kTAM used in this paper satisfies detailed balance within $\mathcal{A}-T$. We prove two facts necessary to show this.

The proof also applies to the case, not considered in this paper, where different tile types have different (but constant) concentrations. For a tile t, $S(t)$ is defined as the relative concentration of its corresponding tile type. Unit concentration is $e^{-G_{mc}}$, such that the concentration of tile type $\mathbf{t}$, $[\mathbf{t}] = S(\mathbf{t})e^{-G_{mc}}$. Additionally, while only equal strength sticky ends are considered in this work, this proof shows that detailed balance applies to a model of self-assembly with arbitrary sticky end strengths.

Lemma 3. *For all reaction pairs $A + t \rightarrow B + t$ and $B \rightarrow A$, $k_f[t][A]_{ss} = k_r[B]_{ss}$, where k_f and k_r are the rates of the respective reactions.*

Proof.

$$\begin{aligned}
k_r[B]_{ss} &= k_f e^{G^\circ(B)-G^\circ(A)}[B]_{ss} \\
&= k_f e^{G^\circ(B)-G^\circ(A)}e^{-G(B)} \\
&= k_f e^{G^\circ(B)-G^\circ(A)}e^{-\left(G^\circ(B)+\sum_{t'\in B} G_{mc}-\ln(S(t'))\right)} \\
&= k_f e^{-G^\circ(A)}e^{-\sum_{t'\in B}\left(G_{mc}-\ln(S(t'))\right)} \\
&= k_f e^{-G^\circ(A)}e^{-\sum_{t'\in A}\left(G_{mc}-\ln(S(t'))\right)}e^{-G_{mc}+\ln(S(t))} \\
&= k_f e^{-G(A)}e^{-G_{mc}+\ln(S(t))} \\
&= k_f[A]_{ss}[t]
\end{aligned}$$

□

Lemma 4. *For reaction pairs $t_1 + t_2 \rightarrow A$ and $A \rightarrow \emptyset$, $k_f[t_1][t_2] = k_r[A]_{ss}$.*

Proof.

$$\begin{aligned}
k_r[A]_{ss} &= k_f e^{G^\circ(A)}[A]_{ss} \\
&= k_f e^{G^\circ(A)}e^{-G(A)} \\
&= k_f e^{G^\circ(A)}e^{-(G^\circ(A)+2G_{mc}-\ln(S(t_1))-\ln(S(t_2)))} \\
&= k_f e^{-G_{mc}+\ln(S(t_1))}e^{-G_{mc}+\ln(S(t_2))} \\
&= k_f[t_1][t_2]
\end{aligned}$$

□

APPENDIX B: STEADY STATE CONCENTRATION AS A BOUND ON ASSEMBLY CONCENTRATION IN A POWERED ACCRETION SELF-ASSEMBLY MODEL

This section contains the proof of Lemma 1: In a powered accretion model of self-assembly where the concentration of all assemblies except for monomers is 0 initially, the concentration of an assembly is bounded by the latter's steady state concentration.

Suppose that this lemma is not true. Then there is a time at which the concentrations of one or more assemblies exceed their values at steady state. Since the concentrations of all assemblies are zero initially, there must be a first time s at which for some assembly A, $[A] = [A]_{ss}$. At this time, the concentrations of all other assemblies are either at or below their respective steady state concentrations. From Section III, the rate of change of $[A]$ is given by the formula

$$\begin{aligned}
\frac{d[A]}{ds} = k_f\Bigg(&\sum_{\substack{A+t\rightarrow B+t,\\ B\rightarrow A\,\in R}} e^{G^\circ(B)-G^\circ(A)}[B] - [A]e^{-G_{mc}} + \\
&\sum_{\substack{B+t\rightarrow A+t,\\ A\rightarrow B\,\in R}} [B]e^{-G_{mc}} - e^{G^\circ(A)-G^\circ(B)}[A] + \\
&\sum_{\substack{t_1+t_2\rightarrow A+t_1+t_2,\\ A\rightarrow\emptyset\in R}} e^{-2G_{mc}} - e^{G^\circ(A)}[A]\Bigg).
\end{aligned}$$

Consider a single term in the second summation, $[B]e^{-G_{mc}} - e^{G^\circ(A)-G^\circ(B)}[A]$, involving some assembly B. We know that $[A]$ has reached its steady state concentration, so $[A] = e^{-G(A)}$. By assumption, $[B] \leq [B]_{ss} = e^{-G(B)}$. Assembly A includes one more tile, t, than does assembly B, so $G^\circ(A) - G^\circ(B) = G(A) - G(B) - G_{mc}$. Therefore,

$$
\begin{aligned}
&[B]e^{-G_{mc}} - e^{G^\circ(A)-G^\circ(B)}[A] \\
&= [B]e^{-G_{mc}} - e^{G(A)-G(B)-G_{mc}}[A] \\
&= [B]e^{-G_{mc}} - e^{G(A)-G(B)-G_{mc}}e^{-G(A)} \\
&= [B]e^{-G_{mc}} - e^{-G(B)}e^{-G_{mc}} \\
&= e^{-G_{mc}}\left([B] - e^{-G(B)}\right) \\
&\leq 0.
\end{aligned}
$$

Similarly, for an assembly B that is a term in the first summation, B has the extra tile t so that $G^\circ(B) - G^\circ(A) = G(B) - G(A) - G_{mc}$. The term can be simplified to

$$
\begin{aligned}
&e^{G^\circ(B)-G^\circ(A)}[B] - [A]e^{-G_{mc}} \\
&= e^{G(B)-G(A)-G_{mc}}[B] - e^{-G(A)}e^{-G_{mc}} \\
&\leq e^{G(B)-G(A)-G_{mc}}e^{-G(B)} - e^{-G(A)}e^{-G_{mc}} \\
&= 0.
\end{aligned}
$$

The terms in the third summation are also non-positive, since

$$
\begin{aligned}
&e^{-2G_{mc}} - e^{G^\circ(A)}[A] \\
&= e^{-2G_{mc}} - e^{G^\circ(A)}e^{-G(A)} \\
&= e^{-2G_{mc}} - e^{G(A)-2G_{mc}} + e^{-G(A)} \\
&= 0.
\end{aligned}
$$

The change in concentration $\frac{d[A]}{ds}(s)$ is composed entirely of terms of this form. Since each of these terms is non-positive, $\frac{d[A]}{ds}(s)$ is non-positive when $[A] = [A]_{ss}$. So $[A]$ can never rise above its steady state value: $[A] \leq [A]_{ss}$.

As in Appendix A, this proof also applies to a model of self-assembly with arbitrary stoichiometry and sticky end strengths.

APPENDIX C: FAST CONVERGENCE OF NUCLEATION RATES AT STEADY STATE

This section contains a proof of Lemma 2 for zig-zag tile sets of width k. Here, we start by re-writing the lemma to use convenient notation to refer to the inner sums within the series for n_k^+, which refer to the rate of spurious nucleation events involving assemblies A of width $k-1$ and length l:

$$
N_p = \sum_{\substack{A+t \to B+t \in R_k^{in} \\ \text{s.t. } length(A)=p}} k_f [A]_{ss} e^{-G_{mc}},
$$

such that $n_k^+ = \sum_{l=1}^{\infty} N_l$. Now, Lemma 2 may be stated as:

Lemma 2. *When $G_{se} > (\ln 10)(k-2) + \ln 4$, $G_{mc} = 2G_{se} - \epsilon$, $0 \leq \epsilon < \frac{1}{2k-3}$ and l is even, then $\sum_{p=l+1}^{\infty} N_p < 2N_l$.*

To prove this lemma, we will prove two sub-lemmas. First,

Lemma 5. *If $G_{se} > (\ln 4)(k-2) + \ln \frac{12}{5}$, $G_{mc} = 2G_{se} - \epsilon$, l is even and $0 \leq \epsilon < \frac{1}{2k-3}$, then $N_{l+1} < \frac{1}{2}N_l$.*

Proof. We will partition the assemblies of length $l+1$ into classes corresponding to assemblies of length l. We will then show the total spurious nucleation rate of reactions containing the assemblies in each class is at least twice as small as the spurious nucleation rate of reactions containing its corresponding assembly. The class of assemblies of length $l+1$ corresponding to an assembly B of length l will be denoted $\hat{B}$.

To assign the assemblies to classes, we introduce a procedure that takes an assembly A of width $k-1$ and length $l+1$, and then "condenses" its right end to yield an assembly B with width $k-1$ and length l. Specifically, A and B are identical except for the last two columns of A and the last column of B; there, if A had a tile in either the ultimate or penultimate column in some particular row, then B will have a tile in its last column in the same row. Recall that for valid zig-zag assemblies, if a tile is present in a particular spot, its tile type is determined by its neighbors – thus, we don't have to specify tile types in our condensation procedure, since there is no choice. Formally, we say that $B = \textbf{condensation}(A)$ if $\forall 0 \leq a < k-1,\ 0 \leq b < l-1:\ \tilde{A}(a,b) = \tilde{B}(a,b)$, and $\forall 0 \leq a < k-1:\ \tilde{B}(a,l-1) = 0$ iff $\tilde{A}(a,l-1) = \tilde{A}(a,l) = 0$. Recall that $\tilde{A}$, the canonical representation of A, begins indexing sites at 0, so the first column has index 0 and the last ($l+1^{\text{st}}$) column has index l. Also note that since l is even, A cannot have a double tile extending into its last column, so no double tiles are condensed.

To see that for every assembly A, $\textbf{condensation}(A)$ is connected, note first that A is an assembly, so it is connected. Furthermore, the connectivity graph of $B = \textbf{condensation}(A)$ (with a vertex for each tile and an edge for each abutting pair) is just a graph-theoretic contraction of the connectivity graph of A that combines any two vertices in the same row of the last two columns of A (then possibly adding some extra edges). Therefore, B remains connected. Thus, each A of width $l+1$ is assigned to a unique, valid assembly B of width l.

Condensation is many-to-one, so there are many assemblies A that condense onto the same smaller assembly B. We assign A to the class corresponding to the assembly $\textbf{condensation}(A)$, *i.e.*, the class

$$
\hat{B} = \{A : \textbf{condensation}(A) = B\}.
$$

For a given assembly B of length l, the elements of $\hat{B}$, all of length $l+1$, can be created by adding p tiles ($1 \leq p \leq$

$k-2$) to the $l+1^{\text{st}}$ column of B, and then removing h tiles ($0 \leq h \leq p-1$) from the l^{th} column.

Imagine making these changes one at a time, say from top to bottom, in each row either moving or adding a tile. For each of the $p-h$ tiles that are added to the $l+1^{\text{st}}$ column where the corresponding tiles in the l^{th} column are not removed, $p-h$ tiles are added to the assembly and no more than $2(p-h)-1$ bonds may be formed. For the h tiles that are moved from the l^{th} to the $l+1^{\text{st}}$ column, no tiles are added, and no more bonds can be created (some might even be lost). Therefore, for each such assembly A,

$$[A]_{ss} \leq e^{-(p-h)G_{mc}} e^{(2(p-h)-1)G_{se}} [B]_{ss}.$$

Let l_A be the number of spurious nucleation reactions that an assembly A is a reactant of. The rate of spurious nucleation events involving assemblies of length $l+1$ is therefore given by:

$$N_{l+1} = \sum_{\substack{A,C \in \mathcal{A} \\ \text{s.t. } A+t \to C+t \in R_k^{in} \\ length(A)=l+1}} k_f [A]_{ss} e^{-G_{mc}}$$

We now partition this sum by summing over all smaller assemblies B, and then for each $A \in \hat{B}$ (recall $\hat{B} = \{A \text{ s.t. } \textbf{condensation}(A) = B\}$) we count the spurious nucleation reactions:

$$= \sum_{\substack{B \in \mathcal{A} \\ \text{s.t. } length(B)=l}} \sum_{\substack{A \in \hat{B}, C \in \mathcal{A} \\ \text{s.t. } A+t \to C+t \in R_k^{in}}} k_f [A]_{ss} e^{-G_{mc}}$$

$$\leq \sum_{\substack{A,B \in \mathcal{A} \\ \text{s.t.} \textbf{condensation}(A)=B \\ length(B)=l}} l_A k_f [A]_{ss} e^{-G_{mc}}$$

Partitioning $\hat{B}$ according to the number of tiles added and moved, and using our inequality for $[A]_{ss}$ in terms of $[B]_{ss}$, we have:

$$\leq \sum_{\substack{B \in \mathcal{A} \\ \text{s.t. } length(B)=l}} \sum_{p=1}^{k-2} \binom{k-2}{p} \sum_{h=0}^{p-1} \binom{p-1}{h}$$
$$l_A k_f [B]_{ss} e^{-(p-h)G_{mc}} e^{(2(p-h)-1)G_{se}} e^{-G_{mc}}$$

Under the conditions of the lemma, $G_{mc} > 2G_{se} - \frac{1}{2k-3}$ so that

$$< \sum_{\substack{B \text{ s.t.} \\ length(B)=l}} \sum_{p=1}^{k-2} \binom{k-2}{p} \sum_{h=0}^{p-1} \binom{p-1}{h}$$
$$l_A k_f [B]_{ss} e^{-2(p-h)G_{se}} e^{\frac{p-h}{2k-3}} e^{(2(p-h)-1)G_{se}} e^{-G_{mc}}$$

$$= \sum_{\substack{B \text{ s.t.} \\ length(B)=l}} \sum_{p=1}^{k-2} \binom{k-2}{p} \sum_{h=0}^{p-1} \binom{p-1}{h}$$
$$l_A k_f [B]_{ss} e^{\frac{(p-h)}{2k-3}} e^{-G_{se}} e^{-G_{mc}}$$

$$= \sum_{\substack{B \text{ s.t.} \\ length(B)=l}} l_A k_f [B]_{ss} \sum_{p=1}^{k-2} \binom{k-2}{p} e^{\frac{p}{2k-3}} e^{-G_{se}}$$
$$\sum_{h=0}^{p-1} \binom{p-1}{h} e^{\frac{-h}{2k-3}} e^{-G_{mc}}$$

Noting that the inner sums are binomial expansions of (e.g. $(1+x)^n = \sum_{i=0}^{n} \binom{n}{i} x^i$) or portions thereof, we can simplify further:

$$= \sum_{\substack{B \text{ s.t.} \\ length(B)=l}} l_A k_f [B]_{ss} \sum_{p=1}^{k-2} \binom{k-2}{p} e^{\frac{p}{2k-3}} e^{-G_{se}}$$
$$(1 + e^{\frac{-1}{2k-3}})^{p-1} e^{-G_{mc}}$$

Since for $k > 2$, $\frac{1}{2} < (1 + e^{\frac{-1}{2k-3}})^{-1} < \frac{3}{5}$,

$$< \sum_{\substack{B \text{ s.t.} \\ length(B)=l}} \frac{3}{5} l_A k_f [B]_{ss} \sum_{p=1}^{k-2} \binom{k-2}{p} e^{\frac{p}{2k-3}} e^{-G_{se}}$$
$$(1 + e^{\frac{-1}{2k-3}})^{p} e^{-G_{mc}}$$

$$< \sum_{\substack{B \text{ s.t.} \\ length(B)=l}} \frac{3}{5} l_A k_f [B]_{ss} \sum_{p=1}^{k-2} \binom{k-2}{p} e^{\frac{p}{2k-3}} 2^p$$
$$e^{-G_{se}} e^{-G_{mc}}$$

$$< \sum_{\substack{B \text{ s.t.} \\ length(B)=l}} \frac{3}{5} l_A k_f [B]_{ss} \left(1 + 2e^{\frac{1}{2k-3}}\right)^{k-2}$$
$$e^{-G_{se}} e^{-G_{mc}}$$

Similarly, for $k > 2$, $(1 + 2e^{\frac{1}{2k-3}}) < 4$, and $l_A < l_B + 1$ since the longer assembly A can have at most one more

spurious nucleation reaction than B, so

$$< \sum_{\substack{B \text{ s.t.} \\ length(B)=l}} \frac{3}{5}(l_B+1)k_f[B]_{ss}e^{\ln(4)(k-2)}e^{-G_{se}}e^{-G_{mc}}$$
$$\leq \sum_{\substack{B \text{ s.t.} \\ length(B)=l}} \frac{6}{5}l_B k_f[B]_{ss}e^{\ln(4)(k-2)}e^{-G_{se}}e^{-G_{mc}}$$

When $G_{se} > \ln(4)(k-2)+\ln(\frac{12}{5})$,

$$< \sum_{\substack{B \text{ s.t.} \\ length(B)=l}} \frac{1}{2}l_B k_f[B]_{ss}e^{-G_{mc}}$$
$$= \frac{1}{2}\sum_{\substack{A+t\to B+t\in R_k^{in} \\ \text{s.t. } length(A)=l}} k_f[A]_{ss}e^{-G_{mc}} = \frac{1}{2}N_l$$

□

The above sub-lemma takes care of the smaller odd terms, but to show that the entire summation is bounded, we show that smaller even terms are also bounded.

Lemma 6. *If $G_{se} > \ln(10)(k-2)+\ln(4)$, $G_{mc} > (2G_{se} - \frac{1}{2k-3})$ and l is even, then $N_{l+2} < \frac{1}{2}N_l$.*

Proof. The proof for this sub-lemma is similar to that for Lemma 5, except that the condensation function is defined so that the presence of a double tile in the $l+1^{\text{st}}$ and $l+2^{\text{nd}}$ columns are taken into account.

Here, we use a procedure that takes an assembly A of width $k-1$ and length $l+2$, and then condenses its right end to yield an assembly B with width $k-1$ and length l. Again, A and B are identical except for the rightmost three columns of A and the last column of B; there, if A had a tile in any of the last three columns in some particular row, then B will have a tile in its last column in the same row. An added detail is that we must now consider that the rightmost two columns of A may contain a double tile; in this case, the rightmost two columns of B must have a double tile also. The double tile may either be on the top or on the bottom; without loss of generality, we assume it is on the bottom, since the other case can be treated identically. Again, the tile types of the new tiles in B are determined by their neighbors. Formally, we say that $B = \textbf{condensation}'(A)$ if

$$\forall 0 \leq a < k-1,\ 0 \leq b < l-1, (a,b) \neq (k-2, l-2):$$
$$\tilde{A}(a,b) = \tilde{B}(a,b), \text{ and}$$
$$\forall 0 \leq a < k-1:\ \tilde{B}(a,l-1) = 0 \text{ iff}$$
$$\tilde{A}(a,l-1) = \tilde{A}(a,l) = \tilde{A}(a,l+1) = 0, \text{ and}$$
$$\tilde{B}(k-2,l-2) = 0 \text{ iff } \tilde{A}(k-2,l-2) = \tilde{A}(k-2,l) = 0.$$

The proof that every assembly A has a connected **condensation′** is virtually identical to the proof in the previous lemma. The rest of the proof is also similar, except that different numbers of tiles may be removed from the $l+1^{\text{st}}$ and $l+2^{\text{nd}}$ columns.

For a given assembly A, creating $\tilde{A}$ from $\tilde{B}$, where $\textbf{condensation}'(A) = B$, requires adding p tiles, $1 \leq p \leq 2k-3$, to the $(l+1)^{\text{st}}$ and $(l+2)^{\text{nd}}$ columns of B, and then removing h tiles, $1 \leq h \leq k-1$, from the l^{th} column.

For each of the $p-h$ tiles that are added to the $(l+1)^{\text{st}}$ column and $(l+2)^{\text{nd}}$ columns where the corresponding tiles in the l^{th} column are not removed, $p-h$ tiles added to the assembly and no more than $2(p-h)-1$ bonds may be formed. For the h tiles that are moved from the l^{th} to the $(l+1)^{\text{st}}$ column or $(l+2)^{\text{nd}}$, no tiles are added, and no more bonds can be created.

Thus, the spurious nucleation rate of these assemblies is given by:

$$N_{l+2} = \sum_{\substack{A+t\to C+t\in R_k^{in} \\ \text{s.t. } length(A)=l+2}} k_f[A]_{ss}e^{-G_{mc}}$$
$$< \sum_{\substack{A,B \\ \text{s.t.}\textbf{condensation}'(A)=B \\ length(B)=l}} l_A k_f[A]_{ss}e^{-G_{mc}}$$
$$< \sum_{\substack{B \text{ s.t.} \\ length(B)=l}} \sum_{p=1}^{2k-3}\binom{2k-3}{p}\sum_{h=0}^{k-2}\binom{k-2}{h} l_A k_f[B]_{ss}e^{-G_{mc}}e^{-(p-h)G_{mc}}e^{(2(p-h)-1)G_{se}}$$

When $G_{mc} > 2G_{se} - \frac{1}{2k-3}$, this similarly reduces to

$$< \sum_{\substack{B \text{ s.t.} \\ length(B)=l}} l_A k_f[B]_{ss}e^{-G_{mc}}e^{-G_{se}} (1+e^{\frac{-1}{2k-3}})^{k-2}(1+e^{\frac{1}{2k-3}})^{2k-3}$$
$$< \sum_{\substack{B \text{ s.t.} \\ length(B)=l}} l_A k_f[B]_{ss}e^{-G_{mc}}e^{-G_{se}} \left((1+e^{\frac{-1}{2k-3}})(1+e^{\frac{1}{2k-3}})^2\right)^{k-2}$$

For $k > 2$, $(1+e^{\frac{-1}{2k-3}})(1+e^{\frac{1}{2k-3}})^2 < 10$, and thus

$$< \sum_{\substack{B \text{ s.t.} \\ length(B)=l}} l_A k_f[B]_{ss}e^{-G_{mc}}e^{-G_{se}}10^{k-2}$$

Therefore, when $G_{se} > \ln(10)(k-2)+\ln(4)$, and recalling

that $l_A \leq l_B + 1$, □

$$
\begin{aligned}
&< \sum_{\substack{B \text{ s.t.} \\ length(B)=l}} \frac{1}{4}(l_B+1)k_f[B]_{ss}e^{-G_{mc}} \\
&< \sum_{\substack{B \text{ s.t.} \\ length(B)=l}} \frac{1}{2}l_B k_f[B]_{ss}e^{-G_{mc}} \\
&= \frac{1}{2}\sum_{\substack{A+t\rightarrow B+t\in R_k^{in} \\ \text{s.t. } length(A)=l}} k_f[A]_{ss}e^{-G_{mc}} = \frac{1}{2}N_l
\end{aligned}
$$

Now, we can combine Lemma 5 and Lemma 6 to derive Lemma 2. If l is even,

$$
\begin{aligned}
\sum_{p=l+1}^{\infty} N_p &= N_{l+1} + N_{l+2} + N_{l+3} + N_{l+4} + \dots \\
&< \frac{1}{2}N_l + \frac{1}{2}N_l + \frac{1}{4}N_l + \frac{1}{4}N_l + \dots \\
&< 2N_l
\end{aligned}
$$

[1] G. M. Whitesides, J. P. Mathias, and C. T. Seto, Science **254**, 1312 (1991).
[2] J.-M. Lehn, Science **260**, 1762 (1993).
[3] E. Winfree, in *DNA Based Computers*, edited by R. J. Lipton and E. B. Baum (American Mathematical Society, Providence, RI, 1996), vol. 27 of *DIMACS*, pp. 199–221.
[4] P. W. K. Rothemund and E. Winfree, in *Symposium on Theory of Computing (STOC)* (ACM, 2000).
[5] D. Soloveichik and E. Winfree, in *DNA Computing 10* (Springer-Verlag, Berlin Heidelberg, 2004).
[6] A. C. Levi and M. Kotrla, J. Phys. : Condens. Matter **9**, 299 (1997).
[7] T.-J. Fu and N. C. Seeman, Biochemistry **32**, 3211 (1993).
[8] T. H. LaBean, H. Yan, J. Kopatsch, F. Liu, E. Winfree, J. H. Reif, and N. C. Seeman, Journal of the American Chemical Society **122**, 1848 (2000).
[9] C. Mao, W. Sun, and N. C. Seeman, Journal of the American Chemical Society **121**, 5437 (1999).
[10] H. Yan, S. H. Park, G. Finkelstein, J. H. Reif, and T. H. LaBean, Science **301**, 1882 (2003).
[11] Y. He, Y. Chen, H. Liu, A. E. Ribbe, and C. Mao, Journal of the American Chemical Society **127**, 12202 (2005).
[12] A. Chworos, I. Severcan, A. Y. Koyfman, P. Weinkam, E. Oroudjev, H. G. Hansma, and L. Jaeger, Science **306**, 2068 (2004).
[13] E. Winfree, F. Liu, L. A. Wenzler, and N. C. Seeman, Nature **394**, 539 (1998).
[14] C. Mao, T. H. LaBean, J. H. Reif, and N. C. Seeman, Nature **407**, 493 (2000).
[15] P. W. K. Rothemund, N. Papadakis, and E. Winfree, PLOS Biology **2**, 424 (2004).
[16] R. D. Barish, P. W. K. Rothemund, and E. Winfree, Nano Lett. **5**, 2586 (2005).
[17] N. C. Seeman, Journal of Biomolecular Structure & Dynamics **8**, 573 (1990).
[18] R. Dirks, M. Lin, E. Winfree, and N. A. Pierce, Nucleic Acids Research **32**, 1392 (2004).
[19] E. Winfree, Tech. Rep. CS-TR:1998.22, Caltech (1998).
[20] M. G. Lagoudakis and T. H. LaBean, in *DNA Based Computers V*, edited by E. Winfree and D. K. Gifford (American Mathematical Society, Providence, RI, 2000), vol. 54 of *DIMACS*, pp. 141–154.
[21] P. W. K. Rothemund, Proceedings of the National Academy of Sciences **97**, 984 (2000).
[22] L. M. Adleman, Q. Cheng, A. Goel, and M.-D. Huang, Symposium on the Theory of Computing (STOC) (2001).
[23] M. Cook, P. W. K. Rothemund, and E. Winfree, in [48], pp. 91–107.
[24] G. Aggarwal, M. H. Goldwasser, M.-Y. Kao, and R. T. Schweller, in *Symposium on Discrete Algorithms* (AMS/SIAM, Providence, RI, 2004), pp. 880–889.
[25] R. Schulman, S. Lee, N. Papadakis, and E. Winfree, in [48], pp. 108–125.
[26] E. Winfree and R. Bekbolatov, in [48], pp. 126–144.
[27] H.-L. Chen and A. Goel, in [49], pp. 62–75.
[28] J. H. Reif, S. Sahu, and P. Yin, in [49], pp. 293–307.
[29] D. Soloveichik and E. Winfree, in *DNA Computing 11* (Springer-Verlay, Berlin Heidelberg, 2005).
[30] D. Sept and J. A. McCammon, Biophysical Journal **81**, 867 (2001).
[31] S. R. Collins, A. Douglass, R. D. Vale, and J. S. Weissman, PLoS Biology **2**, e321 (2004).
[32] R. M. Dirks and N. A. Pierce, Proc. Nat. Acad. Sci. USA **101**, 15275 (2004).
[33] J. F. Kelleher, S. J. Atkinson, and T. D. Pollard, J. Cell. Biol. **10**, 197 (1995).
[34] J. McDonald, American Journal of Physics **30**, 870 (1962).
[35] I. V. Markov, *Crystal Growth for Beginners* (World Scientific Publishing Company, 2003).
[36] V. A. Shneidman, K. A. Jackson, and K. M. Beatty, Journal of Chemical Physics **111**, 6932 (1999).
[37] A. C. Zettlemoyer, ed., *Nucleation* (Marcel Dekker, New York, 1969).
[38] R. Davey and J. Garside, *From Molecules to Crystallizers* (Oxford University Press, Oxford, UK, 2000).
[39] M. Moritz, M. B. Braunfeld, J. W. Sedat, B. Alberts, and D. A. Agard, Nature **378**, 638 (1995).
[40] P. W. K. Rothemund, A. Ekani-Nkodo, N. Papadakis, A. Kumar, D. K. Fygenseon, and E. Winfree, J. Am. Chem. Soc. **126**, 16344 (2004).
[41] J. C. Mitchell, J. R. Harris, J. Malo, J. Bath, and A. J. Turberfield, Journal of the American Chemical Society **126**, 15342 (2004).
[42] D. Liu, S. H. Park, J. H. Reif, and T. H. LaBean, Proc. Nat. Acad. Sci. USA **101**, 717 (2004).
[43] K. A. Dill and S. Bromberg, *Molecular Driving Forces: Statistical Thermodynamics in Chemistry and Biology* (Garland Science, 2002).
[44] R. S. Quartin and J. G. Wetmur, Biochemistry **28**, 1040 (1989).

[45] S. W. Golomb, *Polyominoes* (Princeton University Press, Princeton, N.J., 1994), 2nd ed.
[46] D. T. Gillespie, J. Comput. Phys. **22**, 403 (1976).
[47] H. Yan, T. H. LaBean, L. Feng, and J. H. Reif, Proc. Nat. Acad. Sci. USA **100**, 8103 (2003).
[48] J. Chen and J. Reif, eds., *DNA Computing 9*, vol. LNCS 2943 (Springer-Verlag, Berlin Heidelberg, 2004).
[49] C. Ferretti, G. Mauri, and C. Zandron, eds., *DNA Computing 10*, vol. LNCS 3384 (Springer-Verlag, Berlin Heidelberg, 2005).
[50] In powered models, since $[A]_{ss} = e^{-G(A)}$, free energies that decrease without bound for longer polymers imply that formal steady-state concentrations correspondingly increase without bound. This may seem odd, but it is not problematic; it reflects that providing unbounded materials can lead to an unbounded accumulation of product, and that longer polymers do not achieve steady-state within the time during which the powered model is an appropriate model.
[51] "Imperfect" long assemblies, for example an assembly with irregular width, can be considered as a member of the smallest polymer class that contains a larger, more complete assembly. Since removing tiles from a "perfect" assembly strictly increases its free energy, these "imperfect" assemblies have strictly lower concentrations than their corresponding "perfect" assembly.
[52] The concentration of the class $\mathcal{C}_k$, which at the conditions we consider contains an infinite number of assemblies, is actually infinite at steady state. The inward flux, as we will show, is finite because the concentration of unnucleated assemblies stays finite at steady state, even though there are also an infinite number of unnucleated assemblies.
[53] Because all bonds are unique, for any produced assembly, each potential tile addition either matches the assembly on all sides, such that no errors occur, or matches on no sides, such that the addition does not produce a connected assembly.
[54] It could also be a subset of a rectangular assembly with top instead of bottom tiles, but the free energy of both kinds of assemblies is the same.